

On the stability and convergence of a Galerkin reduced order model (ROM) of compressible flow with solid wall and far-field boundary treatment[‡]

I. Kalashnikova^{1,2,*} and M. F. Barone³

¹*Institute for Computational and Mathematical Engineering, Stanford University, 496 Lomita Mall, Stanford, CA 94305, U.S.A.*

²*Sandia National Laboratories, Aerosciences Department, P.O. Box 5800, MS 0825, Albuquerque, NM 87185, U.S.A.*

³*Sandia National Laboratories, Wind and Water Power Technologies Department, P.O. Box 5800, MS 1124, Albuquerque, NM 87185, U.S.A.*

SUMMARY

A reduced order model (ROM) based on the proper orthogonal decomposition (POD)/Galerkin projection method is proposed as an alternative discretization of the linearized compressible Euler equations. It is shown that the numerical stability of the ROM is intimately tied to the choice of inner product used to define the Galerkin projection. For the linearized compressible Euler equations, a symmetry transformation motivates the construction of a weighted L^2 inner product that guarantees certain stability bounds satisfied by the ROM. Sufficient conditions for well-posedness and stability of the present Galerkin projection method applied to a general linear hyperbolic initial boundary value problem (IBVP) are stated and proven. Well-posed and stable far-field and solid wall boundary conditions are formulated for the linearized compressible Euler ROM using these more general results. A convergence analysis employing a stable penalty-like formulation of the boundary conditions reveals that the ROM solution converges to the exact solution with refinement of both the numerical solution used to generate the ROM and of the POD basis. An *a priori* error estimate for the computed ROM solution is derived, and examined using a numerical test case. Published in 2010 by John Wiley & Sons, Ltd.

Received 20 April 2009; Revised 20 December 2009; Accepted 18 January 2010

KEY WORDS: reduced order model (ROM); proper orthogonal decomposition (POD)/Galerkin projection; linearized compressible Euler equations; numerical stability; error estimates; penalty method

*Correspondence to: I. Kalashnikova, Institute for Computational and Mathematical Engineering, Stanford University, 496 Lomita Mall, Stanford, CA 94305, U.S.A.

†E-mail: irinak@stanford.edu

‡This article is a U.S. Government work and is in the public domain in the U.S.A.

Contract/grant sponsor: United States Department of Energy's National Nuclear Security Administration; contract/grant number: DE-AC04-94AL85000

Contract/grant sponsor: U.S. Department of Defense

Contract/grant sponsor: Engineering Sciences Center at Sandia National Laboratories

1. INTRODUCTION

Despite improved algorithms and powerful supercomputers, computational fluid dynamics (CFD) modeling of unsteady, three-dimensional (3D) fluid flows continues to remain an expensive enterprise. To alleviate the cost of CFD simulation, efforts have been made in the fluid dynamics community to develop low-dimensional models that capture the essential dynamics of a full-order model but that contain far fewer degrees of freedom. These so-called reduced order models (ROMs) allow for the systematic generation of cost-effective representations of complex, large-scale systems, enabling and enhancing the understanding of fluid dynamical systems at a relatively low computational cost.

In the past decade, numerous approaches to building ROMs have been proposed, each with its own inherent strengths. The reduced basis method [1–4], balanced truncation [5, 6] and goal-oriented ROMs [7] are some examples. Recent improvements in model-reduction methodologies have increased these models' potential usefulness, making it possible, for instance, to develop ROMs in predictive settings such as flow controller design [8], shape optimization [9] and aeroelastic stability analysis [10, 11]. Reduced order modeling has also shown considerable potential in real-time applications, that is, applications where real-time simulations must be run using real-time data for on-the-spot decision making, optimization and/or control.

The use of ROMs in a predictive setting raises some fundamental questions regarding their numerical properties, namely consistency, stability and convergence. Many ROM techniques in fluid mechanics are derived from the proper orthogonal decomposition (POD)/Galerkin projection approach [12–14]. In this context, the ROM may be viewed as an alternative discretization of the governing system of partial differential equations (PDEs). The fact that general results pertaining to these properties for POD/Galerkin models of compressible fluid flow are lacking leads to practical limitations of the use of ROMs. A ROM might be stable for a given number of modes but unstable for other choices of basis size; see [15] for an example of this for a POD model.

Stable formulations for ROMs *have* been proposed in some settings. Stability of ROMs for electrical circuit analysis was considered by Freund *et al.* in [16], where it was shown that preservation of passivity, or energy dissipation, of the circuit system guarantees stability of the ROM. In fluid dynamics, Kwasniok [17] recognized the role of energy conservation in ROMs of non-linear, incompressible fluid flow for atmospheric modeling applications, constructing the Galerkin projection so that the non-linear terms in the ROM conserve turbulent kinetic energy or turbulent enstrophy. Other model reduction techniques whose numerical properties have been studied include balanced truncation, a particular form of POD that uses the observability Gramian as an inner product, and least-squares projection. In [5], Rowley and coworkers demonstrated that balanced truncation and balanced POD methods are guaranteed to be stable for linear systems, and also preserve the stability of an equilibrium point at the origin for non-linear systems. It was shown in [7] that least-squares projection can result in a stable ROM.

Convergence analyses and error estimates for POD-based ROMs are complicated by the fact that the span of the POD basis is not complete in the Hilbert space to which the exact solution belongs; it is only complete in the space defined by the CFD solutions used to generate it, and only in an *average* sense. Since the POD basis contains only information of the kinematics of the flow field that were already encoded in the observations, it cannot be expected to contain all the features present in the exact analytical solution. Nevertheless, significant progress has been made in deriving error estimates for fluid dynamic ROMs in recent years. A general convergence result for a least-squares projection approach can be found in [7], where it is shown that as the

reduced basis is enriched, the state error in a steady reduced model is strictly monotonically decreasing. In [18], Rathinam *et al.* provide an error analysis of the POD method applied to a general non-linear dynamical system. In [19, 20], Kunisch and Volkwein develop convergence estimates for ROMs based on a POD approximation in space and a backwards Euler discretization in time for non-linear parabolic systems arising in fluid dynamics, including the incompressible Navier–Stokes equations. In [1, 2], Veroy *et al.* and Nguyen *et al.* derive rigorous *a posteriori* L^2 error bounds for reduced basis approximations of the steady and unsteady viscous Burgers equation (respectively). Veroy, Patera and their collaborators have also developed a convergent method for ROMs of the incompressible Navier–Stokes equations and provided *a posteriori* error estimates [3, 4].

In [21] a POD/Galerkin ROM of compressible inviscid fluid flow over a solid wall boundary was proposed and shown to be numerically stable. The present work provides a rigorous analysis of the stability and convergence properties of this ROM, including effects of boundary conditions. The approach described herein is based on a Galerkin projection of the governing PDEs, in common with the perspective of, for example, [4, 20]. This ‘continuous projection’ approach differs from many POD/Galerkin applications for compressible flow, where the semi-discrete representation of the governing equations is projected, and numerical analysis proceeds from the perspective of a dynamical system of ordinary differential equations. The continuous projection approach has the advantage that the ROM solution behavior can be examined using methods that have traditionally been used for numerical analysis of spectral approximations to PDEs [22].

The remainder of this paper is organized as follows. Section 2 contains an overview of the POD/Galerkin method for model reduction. The governing fluid equations, namely the linearized compressible Euler equations with appropriate far-field and solid wall boundary conditions, are presented in Section 3. In Section 4, an energy stability analysis leads to sufficient conditions for well-posedness of the boundary conditions for a hyperbolic system, and also reveals that the inner product used to define the Galerkin projection is closely tied to the stability of the resulting model. A stable symmetry inner product is defined and a means of implementing the prescribed boundary conditions in a way that preserves the stability of the ROM is developed. *A priori* error estimates for the computed ROM solution relative to the CFD solution and the exact analytical solution are derived in Section 5. Following the analysis is a numerical example that demonstrates the actual convergence properties of the ROM on a problem involving the propagation and reflection of a cylindrical acoustic pulse from two parallel walls in a uniform mean flow (Section 6). Conclusions are offered in Section 7.

2. THE PROPER ORTHOGONAL DECOMPOSITION (POD)/GALERKIN METHOD FOR MODEL REDUCTION

Before turning our attention to the equations of interest, namely the linearized compressible Euler equations (Section 3), we give an overview of the POD/Galerkin method for reducing the order of a complex physical system governed by a general set of PDEs. The approach consists of two steps:

- Step 1:* Calculation of a reduced basis using the POD of an ensemble of flow-field realizations.
- Step 2:* Galerkin projection of the governing (continuous) PDEs onto the basis of POD modes in some appropriate inner product.

In the first step, kinematic information is transferred from the high-fidelity simulation to a relatively small number of modes. Discussed in detail in Lumley [23] and Holmes *et al.* [13], POD is a mathematical procedure that, given an ensemble of data, constructs a basis for that ensemble that is optimal in a well-defined sense. Let $\mathcal{H}(\Omega)$ be a Hilbert space with associated inner product (\cdot, \cdot) , and let $\{\mathbf{u}^k(\mathbf{x})\} \subset \mathcal{H}(\Omega)$ be an ensemble of real vector fields on a domain $\Omega \subset \mathbb{R}^3$. In the present context, the ensemble $\{\mathbf{u}^k(\mathbf{x}) : k=1, \dots, N\}$ is a set of N instantaneous snapshots of a CFD numerical solution field. Mathematically, POD seeks an M -dimensional ($M \ll N$) subspace $\mathcal{H}^M(\Omega) \subset \mathcal{H}(\Omega)$ spanned by the set $\{\phi_j\}$ such that the projection of the difference between the ensemble \mathbf{u}^k and its projection onto $\mathcal{H}^M(\Omega)$ is minimized on average; that is, it seeks the set $\{\phi_i\}$ that solves the following constrained optimization problem:

$$\begin{aligned} \min_{\{\phi_i\}_{i=1}^M} & \quad \langle \|\mathbf{u}^k - \Pi_M \mathbf{u}^k\|^2 \rangle \\ \text{subject to} & \quad (\phi_i, \phi_j) = \delta_{ij}, \quad 1 \leq i \leq M, \quad 1 \leq j \leq i \end{aligned} \tag{1}$$

Here, $\langle \cdot \rangle$ is a discrete averaging operator, e.g. $\langle \|\mathbf{u}^k\|^2 \rangle \equiv 1/N \sum_{k=1}^N \|\mathbf{u}^k\|^2$, and $\Pi_M : \mathcal{H}(\Omega) \rightarrow \mathcal{H}^M(\Omega)$ is an orthogonal projection operator onto the subspace $\mathcal{H}^M(\Omega)$, satisfying properties 1–6 in Section A.2 of the Appendix. It is a well-known result [13, 18, 20, 21] that the solution to (1) reduces to the eigenvalue problem $\mathcal{R}\phi = \lambda\phi$ where $\mathcal{R} \equiv \langle \mathbf{u}^k \otimes \mathbf{u}^k \rangle$ is a self-adjoint and positive semi-definite operator. If one assumes that \mathcal{R} is compact, then there exists a countable set of non-negative eigenvalues λ_i with associated eigenfunctions ϕ_i . It can be shown [13, 23] that the set of M eigenfunctions, or POD modes, $\{\phi_i : i = 1, 2, \dots, M\}$ corresponding to the M largest eigenvalues of \mathcal{R} is precisely the set of $\{\phi_i\}$ that solves (1). The truncated basis $\{\phi_i : i = 1, 2, \dots, M\}$ is optimal in the sense that it describes more energy (on average) of the ensemble than any other linear basis of the same dimension M . Given this basis, the numerical ROM solution \mathbf{u}_M can be represented as a linear combination of POD modes

$$\mathbf{u}_M(\mathbf{x}, t) = \sum_{j=1}^M a_j(t) \phi_j(\mathbf{x}), \tag{2}$$

where the $a_j(t)$ are the so-called ROM coefficients, to be solved for in the ROM.

The second step in constructing a ROM involves projecting the governing system of PDEs onto the POD basis $\{\phi_j\}$ in the inner product (\cdot, \cdot) defining the Hilbert space $\mathcal{H}(\Omega)$. In this step, the full-system dynamics are effectively translated to the implied dynamics of the POD modes. If the governing system of equations for the state variable vector \mathbf{u} has the form

$$\frac{\partial \mathbf{u}}{\partial t} = \mathcal{L}\mathbf{u} + \mathcal{N}_2(\mathbf{u}, \mathbf{u}) + \mathcal{N}_3(\mathbf{u}, \mathbf{u}, \mathbf{u}), \tag{3}$$

where \mathcal{L} is a linear differential operator, and \mathcal{N}_2 and \mathcal{N}_3 are (non-linear) quadratic and cubic operators, respectively, then the Galerkin projection of (3) onto the POD mode ϕ_j for $j = 1, 2, \dots, M$ is

$$\left(\phi_j, \frac{\partial \mathbf{u}_M}{\partial t} \right) = (\phi_j, \mathcal{L}\mathbf{u}_M) + (\phi_j, \mathcal{N}_2(\mathbf{u}_M, \mathbf{u}_M)) + (\phi_j, \mathcal{N}_3(\mathbf{u}_M, \mathbf{u}_M, \mathbf{u}_M)). \tag{4}$$

Substituting the POD decomposition of \mathbf{u} (2) into (4) and applying the orthonormality property of the basis functions ϕ_i gives a set of time-dependent ordinary differential equations (ODEs) in the modal amplitudes (also referred to as the ROM coefficients) that accurately describes the flow dynamics of the full system of PDEs for some limited set of flow conditions:

$$\begin{aligned} \frac{da}{dt} \equiv \dot{a}_j &= \sum_{l=1}^M a_l(\phi_j, \mathcal{L}(\phi_l)) + \sum_{l=1}^M \sum_{m=1}^M a_l a_m(\phi_j, \mathcal{N}_2(\phi_l, \phi_m)) \\ &+ \sum_{l=1}^M \sum_{m=1}^M \sum_{n=1}^M a_l a_m a_n(\phi_j, \mathcal{N}_3(\phi_l, \phi_m, \phi_n)), \end{aligned} \tag{5}$$

for $j = 1, 2, \dots, M$.

We emphasize that, in the ROM presented herein, the Galerkin projection step is applied to the *continuous* system of PDEs. In many applications of reduced order modeling, the *discrete* representation of the equations is projected onto the POD modes. This discrete approach has the advantage that, depending on the implementation, boundary condition terms present in the discretized equation set are inherited by the ROM. Additionally, certain properties of the numerical scheme used to solve the full equations may be inherited by the ROM. The continuous approach, on the other hand, is appealing in that it does not require an intrusive or code-specific implementation. It is also similar in procedure to spectral numerical approximation methods, allowing the use of analysis techniques employed by the spectral methods community [22] (Section 5).

It is also worth remarking that the POD basis $\{\phi_i : i = 1, 2, \dots, M\}$ described above is *not* complete in $\mathcal{H}(\Omega)$. It is, however, complete in an average sense, that is $\langle \|\mathbf{u}^k - \sum_j (\mathbf{u}^k, \phi_j) \phi_j\| \rangle = 0$ for $M = N$. Note that bases other than POD could be used in constructing the ROM using the present model reduction technique, and in fact, the stability results presented in this work do not depend on the choice of basis. To show convergence of the ROM to the exact solution, however, one must choose a basis whose span contains the exact solution.

3. INITIAL BOUNDARY VALUE PROBLEM (IBVP) FOR COMPRESSIBLE FLOW

3.1. Linearized Euler equations for compressible flow

Let $\mathbf{q}^T \equiv (u_1 \ u_2 \ u_3 \ \zeta \ p) \in \mathbb{R}^5$ denote the vector of fluid state variables. Here, u_1, u_2 and u_3 are the x_1 -, x_2 -, and x_3 -components of the velocity vector $\mathbf{u}^T \equiv (u_1 \ u_2 \ u_3)$, p is the fluid pressure, and $\zeta \equiv 1/\rho$ is the specific volume of the fluid (ρ denoting the fluid density).

We take as the governing fluid equations the compressible Euler equations, linearized about a steady base (or mean) state $\bar{\mathbf{q}}$. Splitting the state variable vector \mathbf{q} into a steady mean plus a time-varying fluctuation ($\mathbf{q}(\mathbf{x}, t) = \bar{\mathbf{q}}(\mathbf{x}) + \mathbf{q}'(\mathbf{x}, t)$), this linearization (cf. [24, 25]) results in a system of the form

$$\frac{\partial \mathbf{q}'}{\partial t} + \underbrace{\mathbf{A}_i \frac{\partial \mathbf{q}'}{\partial x_i}}_{\equiv \mathcal{L} \mathbf{q}'} + \mathbf{C} \mathbf{q}' = \mathbf{0}, \tag{6}$$

where

$$\mathbf{A}_1 = \begin{pmatrix} \bar{u}_1 & 0 & 0 & 0 & \bar{\zeta} \\ 0 & \bar{u}_1 & 0 & 0 & 0 \\ 0 & 0 & \bar{u}_1 & 0 & 0 \\ -\bar{\zeta} & 0 & 0 & \bar{u}_1 & 0 \\ \gamma\bar{p} & 0 & 0 & 0 & \bar{u}_1 \end{pmatrix}, \quad \mathbf{A}_2 = \begin{pmatrix} \bar{u}_2 & 0 & 0 & 0 & 0 \\ 0 & \bar{u}_2 & 0 & 0 & \bar{\zeta} \\ 0 & 0 & \bar{u}_2 & 0 & 0 \\ 0 & -\bar{\zeta} & 0 & \bar{u}_2 & 0 \\ 0 & \gamma\bar{p} & 0 & 0 & \bar{u}_2 \end{pmatrix}, \quad (7)$$

$$\mathbf{A}_3 = \begin{pmatrix} \bar{u}_3 & 0 & 0 & 0 & 0 \\ 0 & \bar{u}_3 & 0 & 0 & 0 \\ 0 & 0 & \bar{u}_3 & 0 & \bar{\zeta} \\ 0 & 0 & -\bar{\zeta} & \bar{u}_3 & 0 \\ 0 & 0 & \gamma\bar{p} & 0 & \bar{u}_3 \end{pmatrix}, \quad \mathbf{C} = \begin{pmatrix} \frac{\partial \bar{u}_1}{\partial x_1} & \frac{\partial \bar{u}_1}{\partial x_2} & \frac{\partial \bar{u}_1}{\partial x_3} & \frac{\partial \bar{p}}{\partial x_1} & 0 \\ \frac{\partial \bar{u}_2}{\partial x_1} & \frac{\partial \bar{u}_2}{\partial x_2} & \frac{\partial \bar{u}_2}{\partial x_3} & \frac{\partial \bar{p}}{\partial x_2} & 0 \\ \frac{\partial \bar{u}_3}{\partial x_1} & \frac{\partial \bar{u}_3}{\partial x_2} & \frac{\partial \bar{u}_3}{\partial x_3} & \frac{\partial \bar{p}}{\partial x_3} & 0 \\ \frac{\partial \bar{\zeta}}{\partial x_1} & \frac{\partial \bar{\zeta}}{\partial x_2} & \frac{\partial \bar{\zeta}}{\partial x_3} & -\nabla \cdot \bar{\mathbf{u}} & 0 \\ \frac{\partial \bar{p}}{\partial x_1} & \frac{\partial \bar{p}}{\partial x_2} & \frac{\partial \bar{p}}{\partial x_3} & 0 & \gamma \nabla \cdot \bar{\mathbf{u}} \end{pmatrix}. \quad (8)$$

Here, $\mathbf{0} \in \mathbb{R}^5$ is the zero vector, $\gamma = C_P/C_V$ is the ratio of specific heats and \mathcal{L} is a linear, spatial differential operator. The $\{\mathbf{A}_i : i = 1, 2, 3\}$ matrices are functions of the base flow vector $\bar{\mathbf{q}}$; the matrix \mathbf{C} is a function of $\nabla \bar{\mathbf{q}}$. All the matrices (7)–(8) are independent of time, as the mean flow $\bar{\mathbf{q}}$ is assumed to be steady. In the case of uniform base flow, $\nabla \bar{\mathbf{q}} \equiv \mathbf{0}$, so that $\partial \mathbf{A}_i / \partial x_i \equiv \mathbf{0}$ and $\mathbf{C} \equiv \mathbf{0}$.

It is a well-known fact that the system (6) is hyperbolic. This implies that the tensor $\mathbf{A}_n \equiv \mathbf{A}_1 n_1 + \mathbf{A}_2 n_2 + \mathbf{A}_3 n_3$, for some spatial orientation $\mathbf{n}^T = (n_1 \ n_2 \ n_3)$, is diagonalizable: $\mathbf{A}_n = \mathbf{S} \mathbf{\Lambda}_n \mathbf{S}^{-1}$. Here \mathbf{S} is the matrix that diagonalizes \mathbf{A}_n and $\mathbf{\Lambda}_n$ is a diagonal matrix containing the eigenvalues of \mathbf{A}_n (also referred to as the characteristic speeds):

$$\mathbf{\Lambda}_n = \begin{pmatrix} \bar{u}_n & & & & \\ & \bar{u}_n & & & \\ & & \bar{u}_n & & \\ & & & \bar{u}_n + \bar{c} & \\ & & & & \bar{u}_n - \bar{c} \end{pmatrix}, \quad (9)$$

with $\bar{c} = \sqrt{\gamma \bar{p} \bar{\zeta}}$ denoting the speed of sound. Defining $\mathbf{v}' \equiv \mathbf{S}^{-1} \mathbf{q}'$, the linearized Euler Equations (6) in these so-called ‘characteristic’ variables are[§]

$$\frac{\partial \mathbf{v}'}{\partial t} + \mathbf{S}^{-1} \mathbf{A}_i \mathbf{S} \frac{\partial \mathbf{v}'}{\partial x_i} + \mathbf{S}^{-1} \left[\mathbf{A}_i \frac{\partial \mathbf{S}}{\partial x_i} + \mathbf{C} \mathbf{S} \right] \mathbf{v}' = \mathbf{0}. \tag{11}$$

3.2. Boundary conditions

In typical applications, Ω may contain a fixed or moving solid wall boundary, denoted by $\partial\Omega_W$, over which the fluid flows. Additionally, since the computational domain Ω is by construction finite, in contrast to the infinite physical space on which the initial boundary value problem (IBVP) is defined, boundary conditions should be prescribed on the artificial far-field boundary $\partial\Omega_F$. In this context, it is useful to introduce the following partition of $\partial\Omega$:

$$\partial\Omega = \partial\Omega_F \cup \partial\Omega_W, \quad \partial\Omega_F \cap \partial\Omega_W = \emptyset \tag{12}$$

into a far-field boundary ($\partial\Omega_F$) and a solid wall boundary ($\partial\Omega_W$). With boundary conditions imposed on these two boundaries, an IBVP for the compressible Euler equations (6) has the form

$$\begin{aligned} \frac{\partial \mathbf{q}'}{\partial t} + \mathbf{A}_i \frac{\partial \mathbf{q}'}{\partial x_i} + \mathbf{C} \mathbf{q}' &= \mathbf{0}, & \mathbf{x} \in \Omega, & \quad 0 < t < T, \\ \mathbf{P} \mathbf{q}' &= \mathbf{h}, & \mathbf{x} \in \partial\Omega_W, & \quad 0 < t < T, \\ \mathbf{R} \mathbf{q}' &= \mathbf{g}, & \mathbf{x} \in \partial\Omega_F, & \quad 0 < t < T, \\ \mathbf{q}'(\mathbf{x}, 0) &= \mathbf{f}(\mathbf{x}), & \mathbf{x} \in \Omega. & \end{aligned} \tag{13}$$

Here, \mathbf{P} and \mathbf{h} specify the solid wall boundary conditions, \mathbf{R} and \mathbf{g} specify the far-field boundary conditions and $\mathbf{f}: \Omega \rightarrow \mathbb{R}^5$ is a given vector-valued function of initial data.

3.2.1. Non-reflecting far-field boundary conditions. Without far-field boundary conditions, non-physical reflections of unsteady waves will be observed at the far-field. These unwanted reflections can affect the accuracy of the simulation and possibly lead to numerical instability. An appropriate far-field boundary condition is one that will suppress the reflection of waves from the outer computational boundaries. This is the so-called non-reflecting boundary condition on $\partial\Omega_F$, specified in the characteristic variables \mathbf{v}' . All outgoing unsteady characteristic waves are allowed to exit the flow domain at the far-field boundary without reflection, that is, without being allowed to re-enter the domain through the boundary. This is accomplished by setting the components of \mathbf{v}' corresponding to characteristic waves traveling into Ω (those corresponding to negative eigenvalues

[§]The reader is referred to Section A.1 of the Appendix for explicit expressions of \mathbf{S} , \mathbf{S}^{-1} and \mathbf{v}' . Note that under the uniform base flow assumption, (11) simplifies to

$$\frac{\partial \mathbf{v}'}{\partial t} + \mathbf{S}^{-1} \mathbf{A}_i \mathbf{S} \frac{\partial \mathbf{v}'}{\partial x_i} = \mathbf{0}. \tag{10}$$

of \mathbf{A}_n) to zero:

$$v'_i \leftarrow (v'_f)_i \equiv \begin{cases} 0 & \text{if } \lambda_i < 0 \\ v'_i & \text{if } \lambda_i \geq 0, \end{cases} \quad (14)$$

for $i = 1, \dots, 5$, with $\{\lambda_i : i = 1, \dots, 5\}$ denoting the five eigenvalues of the matrix \mathbf{A}_n (the diagonal entries of \mathbf{A}_n). In matrix form, the far-field condition can be written as

$$\mathbf{R}^S \mathbf{v}' = \mathbf{0} \quad \text{on } \partial\Omega_F, \quad (15)$$

where

$$\mathbf{R}^S \equiv \mathbf{R}\mathbf{S} = \begin{cases} \mathbf{0}_5 & \text{if } \bar{u}_n < -\bar{c} \\ \text{diag}\{0, 0, 0, 0, 1\} & \text{if } -\bar{c} < \bar{u}_n < 0 \\ \text{diag}\{1, 1, 1, 0, 1\} & \text{if } 0 < \bar{u}_n < \bar{c} \\ \mathbf{I}_5 & \text{if } \bar{u}_n > \bar{c}. \end{cases} \quad (16)$$

Here $\mathbf{0}_5$ is the 5×5 zero matrix, \mathbf{I}_5 is the 5×5 identity matrix and $\text{diag}\{\cdot\}$ denotes a diagonal matrix with diagonal entries given by the set in between the brackets. The ranges in (16) correspond to the four cases that can occur at the far-field: supersonic inflow ($\bar{u}_n < -\bar{c}$), subsonic inflow ($-\bar{c} < \bar{u}_n < 0$), subsonic outflow ($0 < \bar{u}_n < \bar{c}$) and supersonic outflow ($\bar{u}_n > \bar{c}$).

3.2.2. Acoustically reflecting (no-penetration) solid wall boundary condition. In applications where the domain Ω contains a stationary or moving solid wall boundary $\partial\Omega_W$, the natural choice of boundary condition at the solid wall boundary is a linearized version of the no-penetration boundary condition, $\mathbf{u} \cdot \mathbf{n} = -\dot{\eta}$:

$$u'_n = -\bar{\mathbf{u}} \cdot \nabla \eta - \dot{\eta} \equiv u'_w \quad \text{on } \partial\Omega_W. \quad (17)$$

Here, η and $\dot{\eta}$ are, respectively, the solid wall displacement and velocity in the $-\mathbf{n}$ direction, with \mathbf{n} denoting the outward unit normal to the solid wall boundary $\partial\Omega_W$ and $u'_n \equiv \mathbf{u}' \cdot \mathbf{n}$. The linearized no-penetration condition (17) is posed in the characteristic variables \mathbf{v}' as an acoustically reflecting condition. Assuming that the base flow satisfies a no-penetration condition at the wall ($\bar{u}_n \equiv 0$ on $\partial\Omega_W$), the characteristic speeds are $\{0, 0, 0, \bar{c}, -\bar{c}\}$. In particular, the fourth characteristic is outgoing and the fifth characteristic is incoming. For a stationary wall, specifying the acoustically reflecting boundary condition amounts to setting the incoming characteristic, v'_5 , equal to the outgoing characteristic, v'_4 . When the wall velocity is $u'_w \equiv u'_w(x, y, t)$, the following relation satisfies (17):

$$v'_5 = v'_4 - 2u'_w \quad \text{on } \partial\Omega_W. \quad (18)$$

That is, (18) and (17) are mathematically equivalent. Equation (18) can be written in matrix form as

$$\mathbf{P}^S \mathbf{v}' = \mathbf{h} \quad \text{on } \partial\Omega_W, \quad (19)$$

with

$$\mathbf{P}^S \equiv \mathbf{P}\mathbf{S} = \begin{pmatrix} 0 & & & & \\ & 0 & & & \\ & & 0 & & \\ & & & 0 & \\ & & & & -1 & 1 \end{pmatrix}, \quad \mathbf{h} = \begin{pmatrix} 0 \\ 0 \\ 0 \\ 0 \\ -2u'_w \end{pmatrix}, \tag{20}$$

or

$$\mathbf{v}' \leftarrow \mathbf{v}'_w \equiv (v'_1 \ v'_2 \ v'_3 \ v'_4 \ v'_4 - 2u'_w)^T \quad \text{on } \partial\Omega_W. \tag{21}$$

A stable and efficient weak implementation of the far-field (14) and solid wall (18) boundary conditions is outlined in Section 4.4.

4. STABLE POD/GALERKIN METHOD FOR HYPERBOLIC SYSTEMS

4.1. Symmetrized compressible Euler equations

A key property of the hyperbolic system (6) is that it is symmetrizable;[‡] that is, there exists a symmetric, positive-definite matrix \mathbf{H} such that $\{\mathbf{H}\mathbf{A}_i : i=1, 2, 3\}$ are all symmetric. The symmetrizer of (6) is given by

$$\mathbf{H} = \begin{pmatrix} \bar{\rho} & 0 & 0 & 0 & 0 \\ 0 & \bar{\rho} & 0 & 0 & 0 \\ 0 & 0 & \bar{\rho} & 0 & 0 \\ 0 & 0 & 0 & \alpha^2 \gamma \bar{\rho}^2 \bar{p} & \bar{\rho} \alpha^2 \\ 0 & 0 & 0 & \bar{\rho} \alpha^2 & \frac{(1 + \alpha^2)}{\gamma \bar{p}} \end{pmatrix}, \tag{22}$$

where α^2 is an arbitrary real, nonzero parameter. Pre-multiplying (6) by the matrix \mathbf{H} yields the following symmetrized system:

$$\frac{\partial(\mathbf{H}\mathbf{q}')}{\partial t} + \mathbf{H}\mathbf{A}_i \frac{\partial \mathbf{q}'}{\partial x_i} + \mathbf{H}\mathbf{C}\mathbf{q}' = \mathbf{0}. \tag{23}$$

Similarly, there exists a positive-definite symmetrizer[‖]

[‡]Among other hyperbolic systems of interest that are symmetrizable are the non-linear Euler equations [26], the compressible Navier–Stokes equations [27], and the shallow water equations [28]. Most hyperbolic systems derived from conservation laws can be symmetrized; see [29, Chapter 6]. A (non-unique) symmetrizer of a matrix (or set of matrices) can be derived using the eigenvectors of the matrix (or matrices), following techniques presented by Gustafsson in [24, 30]. Other symmetric forms of both the linearized Euler and linearized Navier–Stokes equations can be found in Olinger and Sundstrom [25] and in Abarbanel and Gottlieb [31].

[‖]One may check positive-definiteness of \mathbf{Q} by computing its eigenvalues, $\frac{1}{2}\bar{\rho}$, $\bar{\rho}$, $\bar{\rho}$, $\gamma \bar{p}/2c^2$, $\alpha^2 \bar{\rho}^2 \bar{p} \gamma$, which are all >0 if $\alpha \neq 0$.

for the governing system of PDEs in the characteristic variables (11), denoted here by \mathbf{Q} , which has the property that the matrices $\{\mathbf{Q}\mathbf{S}^{-1}\mathbf{A}_i\mathbf{S}; i = 1, 2, 3\}$ are all symmetric:

$$\mathbf{Q} \equiv \mathbf{S}^T \mathbf{H} \mathbf{S} = \begin{pmatrix} \bar{\rho} - \bar{\rho} n_1^2 (1 - \alpha^2 \bar{\rho} \bar{p}) & \bar{\rho} n_1 n_2 (1 - \alpha^2 \bar{\rho} \bar{p}) & -\bar{\rho} n_1 n_3 (1 - \alpha^2 \bar{\rho} \bar{p}) & 0 & 0 \\ \bar{\rho} n_1 n_2 (1 - \alpha^2 \bar{\rho} \bar{p}) & \bar{\rho} - \bar{\rho} n_2^2 (1 - \alpha^2 \bar{\rho} \bar{p}) & \bar{\rho} n_2 n_3 (1 - \alpha^2 \bar{\rho} \bar{p}) & 0 & 0 \\ -\bar{\rho} n_1 n_3 (1 - \alpha^2 \bar{\rho} \bar{p}) & \bar{\rho} n_2 n_3 (1 - \alpha^2 \bar{\rho} \bar{p}) & \bar{\rho} - \bar{\rho} n_3^2 (1 - \alpha^2 \bar{\rho} \bar{p}) & 0 & 0 \\ 0 & 0 & 0 & \frac{1}{2} \bar{\rho} & 0 \\ 0 & 0 & 0 & 0 & \frac{1}{2} \bar{\rho} \end{pmatrix}. \quad (24)$$

4.2. Symmetry inner product and Galerkin projection

As discussed in Section 2, in a POD/Galerkin ROM, the inner product defines the Hilbert space on which the analysis proceeds. The inner product is also a mathematical expression for the energy in the ROM. The majority of POD/Galerkin models for fluid flow use as the governing equation set the incompressible Navier–Stokes equations. For these equations, the natural choice of inner product is the $L^2(\Omega)$ inner product. This is because in these models the solution vector is taken to be the velocity vector \mathbf{u} , so that $\|\mathbf{u}\|_{L^2(\Omega)}$ is a measure of the global kinetic energy in the domain Ω . The $L^2(\Omega)$ inner product is therefore physically sensible: the POD modes optimally represent the kinetic energy present in the ensemble from which they are generated. The same is *not* true for the compressible linearized Euler equations (6) with solution vector \mathbf{q}' as defined in Section 3.1. This fact is discussed at length in [21, 32–34], where it is demonstrated on several test cases that the $L^2(\Omega)$ inner product for these equations does not correspond to an energy integral, meaning if it is selected as the inner product defining the projection, the ROM does not satisfy the energy conservation relation implied by the governing equations.

As we will show in Section 4.3, an appropriate choice of inner product for the system (6) is the so-called ‘symmetry inner product’. For any symmetric positive-definite matrix $\mathbf{M} \in \mathbb{R}^{n \times n}$ and bounded domain $\Omega \subset \mathbb{R}^3$, define the (\mathbf{M}, Ω) -inner product and (\mathbf{M}, Ω) -norm by

$$(\mathbf{v}_1, \mathbf{v}_2)_{(\mathbf{M}, \Omega)} \equiv \int_{\Omega} \mathbf{v}_1^T \mathbf{M} \mathbf{v}_2 \, d\Omega, \quad \|\mathbf{v}\|_{(\mathbf{M}, \Omega)} \equiv \sqrt{(\mathbf{v}, \mathbf{v})_{(\mathbf{M}, \Omega)}}, \quad (25)$$

for $\mathbf{v}_1, \mathbf{v}_2, \mathbf{v} \in \mathbb{R}^n$. The set of functions $\{\mathbf{f}: \Omega \rightarrow \mathbb{R}^n : \|\mathbf{f}\|_{(\mathbf{M}, \Omega)} < \infty\}$ taken together with the (\mathbf{M}, Ω) -inner product forms a Hilbert space. In the context of Equations (6) and (11), we will consider the (\mathbf{H}, Ω) - and (\mathbf{Q}, Ω) -inner products, respectively, with \mathbf{H} defined in (22) and \mathbf{Q} in (24). Given \mathbf{H} (22), the expression for the symmetry inner product with respect to \mathbf{H} over Ω is

$$(\mathbf{q}'^{(1)}, \mathbf{q}'^{(2)})_{(\mathbf{H}, \Omega)} = \int_{\Omega} \left[\bar{\rho} \mathbf{u}'^{(1)} \cdot \mathbf{u}'^{(2)} + \alpha^2 \gamma \bar{\rho}^2 \zeta'^{(1)} \zeta'^{(2)} + \frac{1 + \alpha^2}{\gamma \bar{p}} + \alpha^2 \bar{\rho} (\zeta'^{(2)} p'^{(1)} + \zeta'^{(1)} p'^{(2)}) \right] d\Omega. \quad (26)$$

The (\mathbf{H}, Ω) - and (\mathbf{Q}, Ω) -inner products are equivalent in the sense that

$$(\mathbf{q}'^{(1)}, \mathbf{q}'^{(2)})_{(\mathbf{H}, \Omega)} = (\mathbf{v}'^{(1)}, \mathbf{v}'^{(2)})_{(\mathbf{Q}, \Omega)}, \quad (27)$$

where $\mathbf{v}'^{(1)} = \mathbf{S}^{-1} \mathbf{q}'^{(1)}$, and similarly for $\mathbf{v}'^{(2)}$. Using the relationship (24), it is straightforward to show that, denoting $\phi_k^S \equiv \mathbf{S}^{-1} \phi_k$ and letting Π_M denote an orthogonal projection operator onto the space $\mathcal{H}^M(\Omega)$ (see (1) and Section A.2 of the Appendix),

$$\Pi_M \mathbf{q}' = \sum_{k=1}^M (\phi_k, \mathbf{q}')_{(\mathbf{H}, \Omega)} \phi_k = \mathbf{S} \sum_{k=1}^M (\phi_k^S, \mathbf{v}')_{(\mathbf{Q}, \Omega)} \phi_k^S \equiv \mathbf{S}(\Pi_M \mathbf{v}'). \tag{28}$$

Expanded in its modal basis, the ROM solutions \mathbf{q}'_M and \mathbf{v}'_M are expressed as:

$$\mathbf{q}'_M(\mathbf{x}, t) = \sum_{k=1}^M a_k(t) \phi_k(\mathbf{x}), \quad \mathbf{v}'_M(\mathbf{x}, t) = \sum_{k=1}^M a_k(t) \phi_k^S(\mathbf{x}). \tag{29}$$

The components of the five-vector ϕ_k are denoted ϕ_k^i for $i = 1, \dots, 5$, that is $\phi_k^T = (\phi_k^1 \ \phi_k^2 \ \phi_k^3 \ \phi_k^4 \ \phi_k^5)$. The Galerkin projection of the system of Equations (6) onto the j th POD mode in the (\mathbf{H}, Ω) -inner product is

$$\left(\phi_j, \frac{\partial \mathbf{q}'_M}{\partial t} \right)_{(\mathbf{H}, \Omega)} + \left(\phi_j, \mathbf{A}_i \frac{\partial \mathbf{q}'_M}{\partial x_i} \right)_{(\mathbf{H}, \Omega)} + (\phi_j, \mathbf{C} \mathbf{q}'_M)_{(\mathbf{H}, \Omega)} = 0. \tag{30}$$

Equation (30) gives rise to the following set of M linear ODEs for the time-dependent ROM coefficients $\{a_j(t) : j = 1, 2, \dots, M\}$:

$$\dot{a}_j(t) = - \sum_{k=1}^M a_k(t) \left(\phi_j, \mathbf{A}_i \frac{\partial \phi_k}{\partial x_i} \right)_{(\mathbf{H}, \Omega)} - \sum_{k=1}^M a_k(t) (\phi_j, \mathbf{C} \phi_k)_{(\mathbf{H}, \Omega)}. \tag{31}$$

4.3. Stability of the Galerkin projection in the symmetry inner product

Before beginning a convergence analysis of a ROM for (6), it is crucial to ensure that the IBVP for this system of equations is well-posed, and that the Galerkin projection in the chosen inner product is stable. Theorem 4.3.1 gives sufficient conditions on the boundary conditions for well-posedness of a hyperbolic IBVP of the form (13) and shows that the (\mathbf{H}, Ω) -norm is an energy measure. The proof, given in Section A.5 of the Appendix, is based on the energy approach: an IBVP is well-posed if the energy associated with the analogous homogeneous IBVP (that is, the original IBVP but with homogeneous Dirichlet boundary conditions and no source term) is bounded.**

Theorem 4.3.1

Consider a bounded domain $\Omega \subset \mathbb{R}^3$ with connected boundary $\partial\Omega = \partial\Omega_W \cup \partial\Omega_F$, $\partial\Omega_W \cap \partial\Omega_F = \emptyset$. Let $\mathbf{n}^T \equiv (n_1 \ n_2 \ n_3)$ denote the outward-pointing unit normal vector to $\partial\Omega$, and let $\mathbf{\Lambda}_n \equiv \text{diag}\{\lambda_i\} = \mathbf{S}^{-1} \mathbf{A}_n \mathbf{S}$ be the diagonal matrix containing the eigenvalues of $\mathbf{A}_n \equiv \mathbf{A}_1 n_1 + \mathbf{A}_2 n_2 + \mathbf{A}_3 n_3$. The linear hyperbolic IBVP (13) is well-posed if

$$\sum_{i=1}^5 \lambda_i [(v'_{w0})_i]^2 \geq 0 \quad \text{and} \quad \sum_{i=1}^5 \lambda_i [(v'_{f0})_i]^2 \geq 0, \tag{32}$$

**Refer to Section A.3 of the Appendix for formal definitions of well-posedness, quoted from [35].

with energy estimate

$$\|\mathbf{q}'(\cdot, T)\|_{(\mathbf{H}, \Omega)} \leq e^{\beta T/2} \|\mathbf{f}(\cdot)\|_{(\mathbf{H}, \Omega)}, \tag{33}$$

where β is an upper bound on the eigenvalues of the matrix^{††}

$$\mathbf{B} \equiv \mathbf{H}^{-T/2} \frac{\partial(\mathbf{H}\mathbf{A}_i)}{\partial x_i} \mathbf{H}^{-1/2} - \mathbf{H}^{1/2} \mathbf{C} \mathbf{H}^{-1/2} - (\mathbf{H}^{1/2} \mathbf{C} \mathbf{H}^{-1/2})^T \tag{34}$$

Here, \mathbf{q}'_w (\mathbf{q}'_f) is the state satisfying the boundary conditions on $\partial\Omega_W$ ($\partial\Omega_F$) (13); \mathbf{q}'_{w0} (\mathbf{q}'_{f0}) is the state satisfying the homogenous form of the boundary conditions on $\partial\Omega_W$ ($\partial\Omega_F$), that is, (13) with $\mathbf{h}=\mathbf{0}$ ($\mathbf{g}=\mathbf{0}$); $\mathbf{v}'_{w0}=\mathbf{S}^{-1}\mathbf{q}'_{w0}$, $\mathbf{v}'_{f0}=\mathbf{S}^{-1}\mathbf{q}'_{f0}$.

Proof

Given in Section A.5 of the Appendix. □

An immediate consequence of Theorem 4.3.1 is that, provided the IBVP (13) is well-posed, the Galerkin projection of the ROM approximation \mathbf{q}'_M in the (\mathbf{H}, Ω) -inner product is stable. Replacing ϕ_j in (30) by \mathbf{q}'_M , one obtains

$$\frac{1}{2} \frac{d}{dt} \|\mathbf{q}'_M\|_{(\mathbf{H}, \Omega)}^2 = - \int_{\Omega} \mathbf{q}'_M{}^T \mathbf{H} \mathcal{L} \mathbf{q}'_M \, d\Omega \equiv -(\mathbf{q}'_M, \mathcal{L} \mathbf{q}'_M)_{(\mathbf{H}, \Omega)}, \tag{35}$$

and the analysis proceeds exactly as in (A5)–(A8) but with \mathbf{q}' replaced with \mathbf{q}'_M . It follows that if (32) holds, that is, if the IBVP (13) is well-posed, the semi-discrete Galerkin approximation satisfies the definition of stability (Appendix A.4), with energy estimate

$$\|\mathbf{q}'_M(\cdot, T)\|_{(\mathbf{H}, \Omega)} \leq e^{\beta T/2} \|\mathbf{q}'_M(\cdot, 0)\|_{(\mathbf{H}, \Omega)}, \tag{36}$$

or, in terms of the ROM coefficients, $\sum_{j=1}^M a_j^2(T) \leq \exp\{\beta T\} \sum_{j=1}^M a_j^2(0)$. In the uniform base flow case ($\beta \equiv 0$), (36) reduces to the following strong stability condition:

$$\|\mathbf{q}'_M(\cdot, T)\|_{(\mathbf{H}, \Omega)} \leq \|\mathbf{q}'_M(\cdot, 0)\|_{(\mathbf{H}, \Omega)}, \tag{37}$$

or $\sum_{j=1}^M a_j^2(T) \leq \sum_{j=1}^M a_j^2(0)$ in terms of the ROM coefficients.

The energy estimate (36) establishes the semi-boundedness of the governing spatial differential operator \mathcal{L} defined in (6) in the (\mathbf{H}, Ω) -norm, from which it follows that $(\cdot, \cdot)_{(\mathbf{H}, \Omega)}$ is an energy inner product, with corresponding energy norm $\|\cdot\|_{(\mathbf{H}, \Omega)}$. As a consequence, the Galerkin projection step (30) using the symmetry inner product is guaranteed to produce a stable ROM, provided well-posed boundary conditions are prescribed. We emphasize again that the same is *not* true if the Galerkin projection is performed using the $L^2(\Omega)$ inner product, as exhibited in [21].

Theorem 4.3.1 can be used to show the well-posedness of the IBVP of interest here, namely (13) with \mathbf{R} defined in (16), $\mathbf{g}=\mathbf{0}$, and \mathbf{P} and \mathbf{h} defined in (20) (Corollary 4.3.2), from which the stability of the corresponding Galerkin approximation \mathbf{q}'_M in the (\mathbf{H}, Ω) -inner product follows immediately.

^{††}The shorthand $(\mathbf{M}^{1/2})^T \equiv \mathbf{M}^{T/2}$ is employed, where \mathbf{M} is a positive-definite matrix and $\mathbf{M}^{1/2}$ is its square root factor, so that $\mathbf{M}=\mathbf{M}^{T/2}\mathbf{M}^{1/2}$.

Corollary 4.3.2

Let $\Omega \subset \mathbb{R}^3$ be an open bounded domain with connected boundary $\partial\Omega = \partial\Omega_W \cup \partial\Omega_F$, $\partial\Omega_W \cap \partial\Omega_F = \emptyset$. Assume $\bar{u}_n = 0$ on $\partial\Omega_W$. Then the IBVP (13) with the acoustically reflecting boundary condition (18) on $\partial\Omega_W$ and the non-reflecting condition (14) on $\partial\Omega_F$ is well-posed, with energy estimate given by (33), and the corresponding Galerkin approximation \mathbf{q}'_M is stable with energy estimate (36). In the case of uniform base flow ($\nabla \bar{\mathbf{q}} \equiv 0$), these energy estimates simplify to

$$\|\mathbf{q}'(\cdot, T)\|_{(\mathbf{H}, \Omega)} \leq \|\mathbf{f}(\cdot)\|_{(\mathbf{H}, \Omega)}, \quad \|\mathbf{q}'_M(\cdot, T)\|_{(\mathbf{H}, \Omega)} \leq \|\mathbf{q}'_M(\cdot, 0)\|_{(\mathbf{H}, \Omega)} \tag{38}$$

(that is, $\beta = 0$ in (33) and (36), respectively).

Proof

Substituting the components of (21) into the left-hand side of (32) and using the fact that $\bar{u}_n = 0$ at the wall:

$$\sum_{i=1}^5 \lambda_i [(v'_w)_i]^2 = \bar{c}(v'_4)^2 - \bar{c}(v'_4 - 2u'_w)^2. \tag{39}$$

The right-most expression in (39) is identically zero if $u'_w = 0$, that is, if one considers v'_{w0} . By condition (32), the acoustically reflecting boundary condition (21) on $\partial\Omega_W$ is well-posed. For the far-field non-reflecting boundary condition, observe from (14) that, by construction,

$$\begin{cases} \lambda_i [(v'_{f0})_i]^2 = 0 & \text{if } \lambda_i < 0 \\ \lambda_i [(v'_{f0})_i]^2 \geq 0 & \text{if } \lambda_i \geq 0, \end{cases} \tag{40}$$

as incoming characteristics (those for which $\lambda_i < 0$) are zeroed out whereas outgoing characteristics (those for which $\lambda_i \geq 0$) are left unaltered. Since (32) is satisfied, the far-field condition (40) is well-posed as well. By Theorem 4.3.1, the corresponding energy estimate in the (\mathbf{H}, Ω) -norm is (33). When the base flow is uniform $\partial(\mathbf{H}\mathbf{A}_i)/\partial x_i \equiv \mathbf{0}$ and $\mathbf{C} \equiv \mathbf{0}$, so that $\mathbf{B} \equiv \mathbf{0}$ (34), meaning $\beta = 0$. Thus, (33) reduces to the first expression in (38).

Noting that \mathbf{q}'_M satisfies the same set of equations as \mathbf{q}' , by Theorem 4.3.1, well-posedness of (13) with boundary conditions (18) and (14), shown above using the (\mathbf{H}, Ω) -norm, implies stability of the Galerkin approximation \mathbf{q}'_M in the (\mathbf{H}, Ω) -norm, with energy estimate (36). When $\beta = 0$, this estimate reduces to the second expression in (38). \square

One can see from Corollary 4.3.2 that the uniform base flow assumption yields a clean stability analysis, since the mean flow supports only neutral or decaying disturbances (38). In the non-uniform base flow case, there may exist exponentially growing instabilities, for example, the Kelvin–Helmholtz shear layer instability. It is then difficult to distinguish between natural instability modes supported by the continuous equations and spurious instabilities generated by the numerical discretization.

4.4. Stability preserving implementation of the solid wall and far-field boundary conditions

An efficient implementation of boundary conditions for a Galerkin ROM is through a weak formulation. The system of PDEs (6) is projected onto the j th POD mode in the (\mathbf{H}, Ω) -inner

product, the advection term in (6) is integrated by parts, and the vector specifying the boundary condition is inserted into the boundary integral over $\partial\Omega$ that arises:

$$\begin{aligned} \left(\phi_j, \frac{\partial \mathbf{q}'_M}{\partial t}\right)_{(\mathbf{H}, \Omega)} &= - \underbrace{\int_{\partial\Omega_W} \phi_j^T \mathbf{H} \mathbf{A}_n \mathbf{q}'_w \, dS}_{\equiv I_{W_j}} - \underbrace{\int_{\partial\Omega_F} \phi_j^T \mathbf{H} \mathbf{A}_n \mathbf{q}'_f \, dS}_{\equiv I_{F_j}} \\ &\quad + \int_{\Omega} \left[\frac{\partial}{\partial x_i} [\phi_j^T \mathbf{H} \mathbf{A}_i] - \phi_j^T \mathbf{H} \mathbf{C} \right] \mathbf{q}'_M \, d\Omega. \end{aligned} \tag{41}$$

Performing an additional integration by parts on the first term in the volume integral in (41) yields

$$\int_{\Omega} \frac{\partial}{\partial x_i} [\phi_j^T \mathbf{H} \mathbf{A}_i] \mathbf{q}'_M \, d\Omega = \int_{\partial\Omega_W} \phi_j^T \mathbf{H} \mathbf{A}_n \mathbf{q}'_M \, dS + \int_{\partial\Omega_F} \phi_j^T \mathbf{H} \mathbf{A}_n \mathbf{q}'_M \, dS - \int_{\Omega} \phi_j^T \mathbf{H} \mathbf{A}_i \frac{\partial \mathbf{q}'_M}{\partial x_i} \, d\Omega, \tag{42}$$

so that (41) is equivalent to

$$\begin{aligned} \left(\phi_j, \frac{\partial \mathbf{q}'_M}{\partial t}\right)_{(\mathbf{H}, \Omega)} &= - \left(\phi_j, \mathbf{A}_i \frac{\partial \mathbf{q}'_M}{\partial x_i} + \mathbf{C} \mathbf{q}'_M\right)_{(\mathbf{H}, \Omega)} + \int_{\partial\Omega_W} \phi_j^T \mathbf{H} \mathbf{A}_n (\mathbf{q}'_M - \mathbf{q}'_w) \, dS \\ &\quad + \int_{\partial\Omega_F} \phi_j^T \mathbf{H} \mathbf{A}_n (\mathbf{q}'_M - \mathbf{q}'_f) \, dS. \end{aligned} \tag{43}$$

Inviscid compressible flow conditions are most often implemented in terms of the characteristic variables \mathbf{v}'_w , so that $\mathbf{q}'_w \leftarrow \mathbf{S} \mathbf{v}'_w$ (and similarly for \mathbf{q}'_f) in the appropriate boundary integral in (43). Next, the modal representation $\mathbf{q}'_M \leftarrow \sum_{k=1}^M a_k(t) \phi_k$ is inserted into (43) to yield the following system of M ODEs for the ROM coefficients: for $j = 1, \dots, M$

$$\dot{a}_j(t) = - \sum_{k=1}^M a_k(t) \left(\phi_j, \mathbf{A}_i \frac{\partial \phi_k}{\partial x_i} + \mathbf{C} \phi_k\right)_{(\mathbf{H}, \Omega)} + \sum_{k=1}^M [a_k(t) I_{W_{ujk}} - I_{W_j}] + \sum_{k=1}^M [a_k(t) I_{F_{ujk}} - I_{F_j}], \tag{44}$$

where

$$I_{W_{ujk}} \equiv \int_{\partial\Omega_W} \phi_j^T \mathbf{H} \mathbf{A}_n \phi_k \, dS, \quad I_{F_{ujk}} \equiv \int_{\partial\Omega_F} \phi_j^T \mathbf{H} \mathbf{A}_n \phi_k \, dS, \tag{45}$$

$$I_{W_j} \equiv \int_{\partial\Omega_W} \phi_j^T \mathbf{H} \mathbf{S} \Lambda_n \mathbf{v}'_w \, dS, \quad I_{F_j} \equiv \int_{\partial\Omega_F} \phi_j^T \mathbf{H} \mathbf{S} \Lambda_n \mathbf{v}'_f \, dS. \tag{46}$$

are the boundary integral expressions appearing in the j th ROM equation.^{††} To solve for the ROM coefficients, (44) is advanced in time using a time-integration scheme.

^{††}Explicit expressions of the integrals I_{F_j} in terms of the ROM coefficients and basis functions are given in the Appendix of Barone *et al.* [21].

Remark 1

Note that (43) is the projection of the equations

$$\frac{\partial \mathbf{q}'_M}{\partial t} + \mathbf{A}_i \frac{\partial \mathbf{q}'_M}{\partial x_i} + \mathbf{C} \mathbf{q}'_M = \mathbf{A}_n (\mathbf{q}'_M - \mathbf{q}'_w) \delta_{\partial\Omega_w} + \mathbf{A}_n (\mathbf{q}'_M - \mathbf{q}'_f) \delta_{\partial\Omega_f} \tag{47}$$

onto ϕ_j in the (\mathbf{H}, Ω) inner product, where $\delta_{\partial\Omega}$ is an indicator function marking the boundary $\partial\Omega$:

$$\delta_{\partial\Omega} \equiv \begin{cases} 1 & \text{for } \mathbf{x} \in \partial\Omega \\ 0 & \text{otherwise.} \end{cases} \tag{48}$$

Formulating a boundary condition using the penalty method [22, 36–38] amounts to rewriting the given (generic) boundary value problem as:

$$\begin{cases} \mathcal{L}\mathbf{u} - \mathbf{f} = 0, & \text{in } \Omega \\ \mathbf{B}\mathbf{u} = \mathbf{h}, & \text{on } \partial\Omega \end{cases} \rightarrow \mathcal{L}\mathbf{u} - \mathbf{f} = -\mathbf{\Gamma}(\mathbf{B}\mathbf{u} - \mathbf{h}) \delta_{\partial\Omega} \quad \text{in } \Omega \cup \partial\Omega, \tag{49}$$

where $\mathbf{\Gamma}$ is a matrix of penalty parameters selected such that stability is preserved. The right-hand side of (47) is a penalty-like formulation of the far-field and solid-wall boundary conditions in which the matrix $-\mathbf{A}_n$ plays the role of $\mathbf{\Gamma}$, and will be employed in the subsequent convergence analysis (Section 5). The projection of (47) in the (\mathbf{H}, Ω) inner product is stable by Corollary 4.3.2.

5. CONVERGENCE ANALYSIS AND A PRIORI ERROR ESTIMATES

We are now ready to present *a priori* error estimates for the Galerkin ROM with boundary conditions. These error bounds are derived by adapting techniques traditionally used in the numerical analysis of spectral approximations to PDEs [22] and employ the stable penalty-like formulation exhibited in the previous section (Remark 1). The estimates (Theorem 5.2.3) show that the ROM solution does not blow up in finite time and give insight into the conditions for convergence of the ROM solution to the exact solution. This error bound is computable (Section 6), provided the error in the CFD solution $\|\mathbf{q}'_h - \mathbf{q}'\|_{(\mathbf{H}, \Omega)}$ can be estimated in some way.

5.1. Mathematical preliminaries and formulation

There are three solutions one can speak of in the context of the ROM, belonging to the following three Hilbert spaces, all subspaces of \mathbb{R}^5 :

$$\mathbf{q}'(\mathbf{x}, t) \in \mathcal{H}(\Omega), \quad \mathbf{q}'_h(\mathbf{x}, t) \in \mathcal{H}^h(\Omega), \quad \mathbf{q}'_M(\mathbf{x}, t) \in \mathcal{H}^M(\Omega). \tag{50}$$

The Hilbert spaces $\mathcal{H}(\Omega)$ are essentially weighted $L^2(\Omega)$ spaces, formed by equipping the vector space of functions $\{\mathbf{f}: \Omega \rightarrow \mathbb{R}^5: \|\mathbf{f}\|_{(\mathbf{H}, \Omega)} < \infty\}$ with the (\mathbf{H}, Ω) -inner product (26). \mathbf{q}' denotes the

exact solution to the IBVP for (6), \mathbf{q}'_h denotes the computed CFD solution and \mathbf{q}'_M denotes the computed ROM solution. The exact solution in the characteristic variables $\mathbf{q}' \in \mathcal{H}(\Omega)$ satisfies

$$\begin{aligned} \frac{\partial \mathbf{q}'}{\partial t} + \mathbf{A}_i \frac{\partial \mathbf{q}'}{\partial x_i} + \mathbf{C}\mathbf{q}' &= \mathbf{0}, & \mathbf{x} \in \Omega, & \quad 0 < t < T, \\ \mathbf{q}' - \mathbf{q}'_w &= \mathbf{0}, & \mathbf{x} \in \partial\Omega_W, & \quad 0 < t < T, \\ \mathbf{q}' - \mathbf{q}'_f &= \mathbf{0}, & \mathbf{x} \in \partial\Omega_F, & \quad 0 < t < T, \\ \mathbf{q}'(\mathbf{x}, 0) &= \mathbf{f}(\mathbf{x}), & \mathbf{x} \in \Omega. & \end{aligned} \tag{51}$$

Here $\mathbf{f}: \Omega \rightarrow \mathbb{R}^5$ is a given vector-valued function of initial data, $\mathbf{q}'_w = \mathbf{S}\mathbf{v}'_w$ is the vector defining the solid-wall boundary condition (21) and $\mathbf{q}'_f = \mathbf{S}\mathbf{v}'_f$ is the vector defining the far-field boundary condition (14). The CFD solution $\mathbf{q}'_h(\mathbf{x}, t) \in \mathcal{H}^h(\Omega) \subset \mathbb{R}^5$ as defined in (50) is piecewise continuous in space and in time. In the numerical implementation, the CFD solution \mathbf{q}'_h is considered as semi-discrete: that is, it is discrete in space and continuous in time. The CFD data may be generated using virtually any relevant numerical method.^{§§} Motivated primarily by Funaro and Gottlieb [22], the ROM solution, \mathbf{q}'_M , is defined as the solution to the following IBVP with a penalty-type boundary treatment for $0 < t < T$:

$$\begin{aligned} \frac{\partial \mathbf{q}'_M}{\partial t} + \mathbf{A}_i \frac{\partial \mathbf{q}'_M}{\partial x_i} + \mathbf{C}\mathbf{q}'_M &= \mathbf{A}_n[\mathbf{q}'_M - \mathbf{q}'_w] \delta_{\partial\Omega_W} + \mathbf{A}_n[\mathbf{q}'_M - \mathbf{q}'_f] \delta_{\partial\Omega_F}, & \mathbf{x} \in \Omega \cup \partial\Omega_W \cup \partial\Omega_F, \\ \mathbf{q}'_M(\mathbf{x}, 0) &= \mathbf{f}(\mathbf{x}), & \mathbf{x} \in \Omega. \end{aligned} \tag{52}$$

The right-hand side of (52) involves the penalty-like formulation of the boundary conditions exhibited in Section 4.4. Its Galerkin projection in the (\mathbf{H}, Ω) inner product is stable by Remark 1.

Let $\mathbf{q}' \in \mathcal{H}(\Omega)$ and $\mathbf{q}'_M \in \mathcal{H}^M(\Omega)$. Let $\mathbf{e} \equiv \Pi_M \mathbf{q}' - \mathbf{q}'_M$, where $\Pi_M: \mathcal{H}(\Omega) \rightarrow \mathcal{H}^M(\Omega)$ is an orthogonal projection operator satisfying properties 1–6 listed in Section A.2 of the Appendix. In the context of the ROM, the natural definition of Π_M is (28). Applying Π_M to (51) gives

$$\begin{aligned} \frac{\partial(\Pi_M \mathbf{q}')}{\partial t} + \mathbf{A}_i \frac{\partial(\Pi_M \mathbf{q}')}{\partial x_i} + \mathbf{C}\Pi_M \mathbf{q}' + \left[\Pi_M \left(\mathbf{A}_i \frac{\partial \mathbf{q}'}{\partial x_i} + \mathbf{C}\mathbf{q}' \right) - \left(\mathbf{A}_i \frac{\partial(\Pi_M \mathbf{q}')}{\partial x_i} + \mathbf{C}\Pi_M \mathbf{q}' \right) \right] &= \mathbf{0}, & \mathbf{x} \in \Omega, \\ \Pi_M(\mathbf{q}' - \mathbf{q}'_w) &= \mathbf{0}, & \mathbf{x} \in \partial\Omega_W, \\ \Pi_M(\mathbf{q}' - \mathbf{q}'_f) &= \mathbf{0}, & \mathbf{x} \in \partial\Omega_F, \\ \Pi_M \mathbf{q}'(\mathbf{x}, 0) &= \Pi_M \mathbf{f}(\mathbf{x}), & \mathbf{x} \in \Omega. \end{aligned} \tag{53}$$

^{§§}In the current implementation, the CFD data are represented as piecewise linear fields. Discretizing the domain Ω into n grid-points and denoting the CFD solution at the i th grid-point as $\mathbf{q}'_h(\mathbf{x}_i, t)$, the discretized CFD solution vector is then $\hat{\mathbf{q}}'_h(t) \equiv (\mathbf{q}'_h(\mathbf{x}_1, t) \dots \mathbf{q}'_h(\mathbf{x}_n, t))^T$. The reader is referred to [21] for a thorough discussion of the finite element representation of the CFD solution.

for $0 < t < T$. Now, subtracting (52) from (53), one has that

$$\begin{aligned} \frac{\partial \mathbf{e}}{\partial t} + \mathbf{A}_i \frac{\partial \mathbf{e}}{\partial x_i} + \mathbf{C}\mathbf{e} + \mathbf{w} &= \mathbf{A}_n[\mathbf{e} - \mathbf{e}_w] \delta_{\partial\Omega_W} + \mathbf{A}_n[\mathbf{e} - \mathbf{e}_f] \delta_{\partial\Omega_F}, \quad \mathbf{x} \in \Omega \cup \partial\Omega_W \cup \partial\Omega_F, \quad 0 < t < T, \\ \mathbf{e}(\mathbf{x}, 0) &= \Pi_M \mathbf{f}(\mathbf{x}) - \mathbf{f}(\mathbf{x}), \quad \mathbf{x} \in \Omega, \end{aligned} \tag{54}$$

where $\mathbf{e}_w \equiv \Pi_M \mathbf{q}'_w - \mathbf{q}'_w$, $\mathbf{e}_f \equiv \Pi_M \mathbf{q}'_f - \mathbf{q}'_f$ and

$$\mathbf{w} \equiv \Pi_M \left(\mathbf{A}_i \frac{\partial \mathbf{q}'}{\partial x_i} + \mathbf{C}\mathbf{q}' \right) - \left(\mathbf{A}_i \frac{\partial (\Pi_M \mathbf{q}')}{\partial x_i} + \mathbf{C}\Pi_M \mathbf{q}' \right) = \Pi_M(\mathcal{L}\mathbf{q}') - \mathcal{L}(\Pi_M \mathbf{q}'). \tag{55}$$

5.2. Error estimates in the $\mathcal{H}(\Omega)$ Hilbert space

In the upcoming proofs, the shorthand

$$\mathbf{v}'_M \equiv (v'_{1,M} \ v'_{2,M} \ v'_{3,M} \ v'_{3,M} \ v'_{5,M})^T, \quad \Pi_M \mathbf{v}' \equiv (v'_{1,\Pi} \ v'_{2,\Pi} \ v'_{3,\Pi} \ v'_{4,\Pi} \ v'_{5,\Pi})^T \tag{56}$$

will be employed, where, as expected $\mathbf{v}'_M = \mathbf{S}^{-1} \mathbf{q}'_M$ and, from (28), $\Pi_M \mathbf{v}' = \mathbf{S}^{-1} \Pi_M \mathbf{q}'$ so that

$$\mathbf{e} = \mathbf{S}(\Pi_M \mathbf{v}' - \mathbf{v}'_M) \equiv \mathbf{S}\mathbf{e}^S, \tag{57}$$

and similarly for \mathbf{e}_w and \mathbf{e}_f . We begin by proving the following two lemmas.

Lemma 5.2.1

Let $\mathbf{q}' \in \mathcal{H}(\Omega)$ satisfy (51) and let $\mathbf{q}'_M \in \mathcal{H}^M(\Omega)$ satisfy (52). Denote $\mathbf{e} \equiv \Pi_M \mathbf{q}' - \mathbf{q}'_M$, $\mathbf{e}_w \equiv \Pi_M \mathbf{q}'_w - \mathbf{q}'_w$, $\mathbf{e}_f \equiv \Pi_M \mathbf{q}'_f - \mathbf{q}'_f$ with \mathbf{e} satisfying (54). Then

$$\|\mathbf{e}(\cdot, T)\|_{(\mathbf{H},\Omega)}^2 \leq \exp\{1 + \beta T\} \|\mathbf{e}(\cdot, 0)\|_{(\mathbf{H},\Omega)}^2 + T \int_0^T \|\mathbf{w}(\cdot, t)\|_{(\mathbf{H},\Omega)}^2 dt, \tag{58}$$

where \mathbf{w} is defined in (55) and β is an upper bound on the eigenvalues of the matrix \mathbf{B} defined in (34).

Proof

Begin with (54). Taking the inner product with \mathbf{e} , integrating by parts and exploiting the symmetry property of the $\mathbf{H}\mathbf{A}_i$ matrices gives

$$\begin{aligned} \frac{1}{2} \frac{d}{dt} \|\mathbf{e}\|_{(\mathbf{H},\Omega)}^2 &= \frac{1}{2} \int_{\Omega} \mathbf{e}^T \mathbf{H}^{T/2} \mathbf{B} \mathbf{H}^{1/2} \mathbf{e} d\Omega + \int_{\partial\Omega_W} \mathbf{e}^T \mathbf{H} \mathbf{A}_n \left(\frac{1}{2} \mathbf{e} - \mathbf{e}_w \right) dS \\ &\quad + \int_{\partial\Omega_F} \mathbf{e}^T \mathbf{H} \mathbf{A}_n \left(\frac{1}{2} \mathbf{e} - \mathbf{e}_f \right) dS - (\mathbf{w}, \mathbf{e})_{(\mathbf{H},\Omega)} \\ &\leq \frac{1}{2} \beta \|\mathbf{e}\|_{(\mathbf{H},\Omega)}^2 + \int_{\partial\Omega_W} \mathbf{e}^T \mathbf{H} \mathbf{A}_n \left(\frac{1}{2} \mathbf{e} - \mathbf{e}_w \right) dS + \int_{\partial\Omega_F} \mathbf{e}^T \mathbf{H} \mathbf{A}_n \left(\frac{1}{2} \mathbf{e} - \mathbf{e}_f \right) dS \\ &\quad - (\mathbf{w}, \mathbf{e})_{(\mathbf{H},\Omega)}, \end{aligned} \tag{59}$$

where β is an upper bound on the eigenvalues of the matrix \mathbf{B} defined in (34). By (57) and employing the relation (24),

$$\int_{\partial\Omega_W} \mathbf{e}^T \mathbf{H} \mathbf{A}_n \left(\frac{1}{2} \mathbf{e} - \mathbf{e}_w \right) dS = \int_{\partial\Omega_W} (\mathbf{e}^S)^T \mathbf{Q} \mathbf{\Lambda}_n \left(\frac{1}{2} \mathbf{e}^S - \mathbf{e}_w^S \right) dS, \tag{60}$$

$$\int_{\partial\Omega_F} \mathbf{e}^T \mathbf{H} \mathbf{A}_n \left(\frac{1}{2} \mathbf{e} - \mathbf{e}_f \right) dS = \int_{\partial\Omega_F} (\mathbf{e}^S)^T \mathbf{Q} \mathbf{\Lambda}_n \left(\frac{1}{2} \mathbf{e}^S - \mathbf{e}_f^S \right) dS. \tag{61}$$

Exploiting the fact that \mathbf{Q} is symmetric positive definite and $\mathbf{Q} \mathbf{\Lambda}_n = \mathbf{\Lambda}_n \mathbf{Q}$, as in the proof of Theorem 4.3.1 (Section A.5 of the Appendix), (59) can be written as:

$$\begin{aligned} \frac{1}{2} \frac{d}{dt} \|\mathbf{e}\|_{(\mathbf{H}, \Omega)}^2 &\leq \int_{\partial\Omega_W} \mathbf{Q}^{T/2} \left[\sum_{i=1}^5 \lambda_i \left(\frac{1}{2} (e_i^S)^2 - e_i^S [(e_w^S)_i] \right) \right] \mathbf{Q}^{1/2} dS \\ &\quad + \int_{\partial\Omega_F} \mathbf{Q}^{T/2} \left[\sum_{i=1}^5 \lambda_i \left(\frac{1}{2} (e_i^S)^2 - e_i^S [(e_f^S)_i] \right) \right] \mathbf{Q}^{1/2} dS - (\mathbf{w}, \mathbf{e})_{(\mathbf{H}, \Omega)} \\ &\quad + \frac{1}{2} \beta \|\mathbf{e}\|_{(\mathbf{H}, \Omega)}^2. \end{aligned} \tag{62}$$

Then, from the solid wall boundary condition (21) and employing the shorthand (56),

$$\begin{aligned} \sum_{i=1}^5 \lambda_i \left(\frac{1}{2} (e_i^S)^2 - e_i^S [(e_w^S)_i] \right) &= \bar{c} \left[\frac{1}{2} (e_4^S)^2 - e_4^S (e_w^S)_4 - \frac{1}{2} (e_5^S)^2 + e_5^S (e_w^S)_5 \right] \\ &= \frac{1}{2} \bar{c} [-(v'_{4,\Pi} - v'_{4,M})^2 - (v'_{5,\Pi} - v'_{5,M})^2 \\ &\quad + 2(v'_{5,\Pi} - v'_{5,M})(v'_{4,\Pi} - v'_{4,M})]. \end{aligned} \tag{63}$$

By Young’s inequality,

$$2(v'_{5,\Pi} - v'_{5,M})(v'_{4,\Pi} - v'_{4,M}) \leq (v'_{4,\Pi} - v'_{4,M})^2 + (v'_{5,\Pi} - v'_{5,M})^2. \tag{64}$$

Substituting this bound into the right-hand side of (63) gives

$$\sum_{i=1}^5 \lambda_i \left(\frac{1}{2} (e_i^S)^2 - e_i^S [(e_w^S)_i] \right) \leq 0. \tag{65}$$

Equation (65) implies that the term (60) can be omitted from (62), as it is non-positive. Turning our attention to the integral over $\partial\Omega_F$, remark that, from (14),

$$(e_f^S)_i = \begin{cases} 0 & \text{if } \lambda_i < 0, \\ e_i^S & \text{if } \lambda_i \geq 0. \end{cases} \tag{66}$$

It follows that

$$\sum_{i=1}^5 \lambda_i \left(\frac{1}{2} (e_i^S)^2 - e_i^S [(e_f^S)_i] \right) = -\frac{1}{2} \sum_{i=1}^5 \sum_{\lambda_i \geq 0} \lambda_i (e_i^S)^2 \leq 0, \tag{67}$$

which implies that the expression (61) is also non-positive and can be omitted from (62). Thus, (62) simplifies to, invoking Young’s inequality,

$$\frac{d}{dt} \|\mathbf{e}\|_{(\mathbf{H},\Omega)}^2 \leq -2(\mathbf{w}, \mathbf{e})_{(\mathbf{H},\Omega)} + \beta \|\mathbf{e}\|_{(\mathbf{H},\Omega)}^2 \leq \left(\frac{1}{T} + \beta\right) \|\mathbf{e}\|_{(\mathbf{H},\Omega)}^2 + T \|\mathbf{w}\|_{(\mathbf{H},\Omega)}^2. \tag{68}$$

Applying Gronwall’s Lemma to (68) gives (58). □

Lemma 5.2.2

Let \mathbf{w} be as defined in (55). Let $\mathbf{q}'_h \in \mathcal{H}^h(\Omega)$ be the CFD solution. Then the following bound holds

$$\begin{aligned} \|\mathbf{w}(\cdot, T)\|_{(\mathbf{H},\Omega)}^{\text{avg}} &\leq \|\Pi_M(\mathcal{L}\{\mathbf{q}' - \mathbf{q}'_h\})(\cdot, T)\|_{(\mathbf{H},\Omega)}^{\text{avg}} + \|\mathcal{L}\{\Pi_M(\mathbf{q}' - \mathbf{q}'_h)\}(\cdot, T)\|_{(\mathbf{H},\Omega)}^{\text{avg}} \\ &\quad + \|\{\Pi_M(\mathcal{L}\mathbf{q}'_h) - \mathcal{L}(\Pi_M\mathbf{q}'_h)\}(\cdot, T)\|_{(\mathbf{H},\Omega)}^{\text{avg}}, \end{aligned} \tag{69}$$

where

$$\|\mathbf{q}'\|_{(\mathbf{H},\Omega)}^{\text{avg}} \equiv \sqrt{\frac{1}{T} \int_0^T \|\mathbf{q}'\|_{(\mathbf{H},\Omega)}^2 dt}. \tag{70}$$

is the ‘time-averaged’ (\mathbf{H}, Ω) -norm.

Proof

Let $\mathbf{q}'_h \in \mathcal{H}^h(\Omega)$ be the CFD solution. From (55) and applying the Minkowski inequality,

$$\begin{aligned} \|\mathbf{w}(\cdot, T)\|_{(\mathbf{H},\Omega)}^{\text{avg}} &= \left(\frac{1}{T} \int_0^T \|\Pi_M(\mathcal{L}\mathbf{q}' - \mathcal{L}(\Pi_M\mathbf{q}'))\|_{(\mathbf{H},\Omega)}^2 dt\right)^{1/2} \\ &= \left(\frac{1}{T} \int_0^T \|\Pi_M(\mathcal{L}\mathbf{q}' - \Pi_M(\mathcal{L}\mathbf{q}'_h) + \Pi_M(\mathcal{L}\mathbf{q}'_h) - \mathcal{L}(\Pi_M\mathbf{q}'))\right. \\ &\quad \left.+ \mathcal{L}(\Pi_M\mathbf{q}'_h) - \mathcal{L}(\Pi_M\mathbf{q}'_h)\|_{(\mathbf{H},\Omega)}^2 dt\right)^{1/2} \\ &\leq \sqrt{\frac{1}{T} \int_0^T \|\Pi_M(\mathcal{L}\{\mathbf{q}' - \mathbf{q}'_h\})\|_{(\mathbf{H},\Omega)}^2 dt} + \sqrt{\frac{1}{T} \int_0^T \|\mathcal{L}\{\Pi_M(\mathbf{q}' - \mathbf{q}'_h)\}\|_{(\mathbf{H},\Omega)}^2 dt} \\ &\quad + \sqrt{\frac{1}{T} \int_0^T \|\Pi_M(\mathcal{L}\mathbf{q}'_h) - \mathcal{L}(\Pi_M\mathbf{q}'_h)\|_{(\mathbf{H},\Omega)}^2 dt}. \end{aligned} \tag{71}$$

Recognizing the expressions in (71) as time-averaged (\mathbf{H}, Ω) -norms gives (69). □

Lemmas 5.2.1 and 5.2.2 lead to the following theorem, in which the error in the ROM solution $\|(\mathbf{q}' - \mathbf{q}'_M)(\cdot, T)\|_{(\mathbf{H},\Omega)}$ is bounded in the space $\mathcal{H}(\Omega)$.

Theorem 5.2.3

Let $\mathbf{q}' \in \mathcal{H}(\Omega)$ satisfy (51) and $\mathbf{q}'_M \in \mathcal{H}^M(\Omega)$ satisfy (52). Let $\Pi_M: \mathcal{H}(\Omega) \rightarrow \mathcal{H}^M(\Omega)$ be an orthogonal projection operator satisfying properties 1–6 of Section A.2 of the Appendix, and let $\mathbf{e} = \Pi_M \mathbf{q}' - \mathbf{q}'_M$. Let $\mathbf{q}'_h \in \mathcal{H}^h(\Omega)$ be the CFD solution. Then

$$\begin{aligned} \|(\mathbf{q}' - \mathbf{q}'_M)(\cdot, T)\|_{(\mathbf{H}, \Omega)} &\leq \exp\left\{\frac{1}{2}(1 + \beta T)\right\} \|\mathbf{e}(\cdot, 0)\|_{(\mathbf{H}, \Omega)} + \|(\mathbf{q}'_h - \Pi_M \mathbf{q}'_h)(\cdot, T)\|_{(\mathbf{H}, \Omega)} \\ &\quad + T \|\{\Pi_M(\mathcal{L} \mathbf{q}'_h) - \mathcal{L}(\Pi_M \mathbf{q}'_h)\}(\cdot, T)\|_{(\mathbf{H}, \Omega)}^{\text{avg}} + 2\|(\mathbf{q}' - \mathbf{q}'_h)(\cdot, T)\|_{(\mathbf{H}, \Omega)} \\ &\quad + T \|\Pi_M(\mathcal{L}\{\mathbf{q}' - \mathbf{q}'_h\})(\cdot, T)\|_{(\mathbf{H}, \Omega)}^{\text{avg}} + T \|\mathcal{L}\{\Pi_M(\mathbf{q}' - \mathbf{q}'_h)\}(\cdot, T)\|_{(\mathbf{H}, \Omega)}^{\text{avg}}, \end{aligned} \tag{72}$$

where β is an upper bound on the eigenvalues of the matrix \mathbf{B} defined in (34).

Proof

Note that $\mathbf{q}' - \mathbf{q}'_M = \mathbf{q}' - \Pi_M \mathbf{q}' + \Pi_M \mathbf{q}' - \mathbf{q}'_M = (\mathbf{q}' - \Pi_M \mathbf{q}') + \mathbf{e}$. By the triangle inequality,

$$\|(\mathbf{q}' - \mathbf{q}'_M)(\cdot, T)\|_{(\mathbf{H}, \Omega)} \leq \|(\Pi_M \mathbf{q}' - \mathbf{q}')(\cdot, T)\|_{(\mathbf{H}, \Omega)} + \|\mathbf{e}(\cdot, T)\|_{(\mathbf{H}, \Omega)}, \tag{73}$$

where $\|\mathbf{e}(\cdot, T)\|_{(\mathbf{H}, \Omega)}^2$ is bounded according to (58). Applying the triangle inequality again and using the fact that $\|\Pi_M\|_{(\mathbf{H}, \Omega)} = 1$, Π_M being an orthogonal projector (see Section A.2 of the Appendix):

$$\begin{aligned} \|\mathbf{q}' - \Pi_M \mathbf{q}'\|_{(\mathbf{H}, \Omega)} &= \|\mathbf{q}' - \Pi_M \mathbf{q}' + \mathbf{q}'_h - \Pi_M \mathbf{q}'_h - \mathbf{q}'_h + \Pi_M \mathbf{q}'_h\|_{(\mathbf{H}, \Omega)} \\ &\leq \|\mathbf{q}'_h - \Pi_M \mathbf{q}'_h\|_{(\mathbf{H}, \Omega)} + \|\mathbf{q}' - \mathbf{q}'_h\|_{(\mathbf{H}, \Omega)} + \|\Pi_M(\mathbf{q}' - \mathbf{q}'_h)\|_{(\mathbf{H}, \Omega)} \\ &\leq \|\mathbf{q}'_h - \Pi_M \mathbf{q}'_h\|_{(\mathbf{H}, \Omega)} + (1 + \|\Pi_M\|_{(\mathbf{H}, \Omega)}) \|\mathbf{q}' - \mathbf{q}'_h\|_{(\mathbf{H}, \Omega)} \\ &= \|\mathbf{q}'_h - \Pi_M \mathbf{q}'_h\|_{(\mathbf{H}, \Omega)} + 2\|\mathbf{q}' - \mathbf{q}'_h\|_{(\mathbf{H}, \Omega)}. \end{aligned} \tag{74}$$

Substituting (74) into (73) gives

$$\|(\mathbf{q}' - \mathbf{q}'_M)(\cdot, T)\|_{(\mathbf{H}, \Omega)} \leq \|(\mathbf{q}'_h - \Pi_M \mathbf{q}'_h)(\cdot, T)\|_{(\mathbf{H}, \Omega)} + 2\|(\mathbf{q}' - \mathbf{q}'_h)(\cdot, T)\|_{(\mathbf{H}, \Omega)} + \|\mathbf{e}(\cdot, T)\|_{(\mathbf{H}, \Omega)}. \tag{75}$$

Using the fact that $\int_{\Omega} f^2 \, d\Omega \leq (\int_{\Omega} |f| \, d\Omega)^2$ and the inequalities (58) and (69), we have

$$\begin{aligned} \|\mathbf{e}(\cdot, T)\|_{(\mathbf{H}, \Omega)} &\leq \{e^{1+\beta T} \|\mathbf{e}(\cdot, 0)\|_{(\mathbf{H}, \Omega)}^2 + T^2 (\|\mathbf{w}(\cdot, t)\|_{(\mathbf{H}, \Omega)}^{\text{avg}})^2\}^{1/2} \\ &\leq e^{\frac{1}{2}(1+\beta T)} \|\mathbf{e}(\cdot, 0)\|_{(\mathbf{H}, \Omega)} + T \|\mathbf{w}(\cdot, T)\|_{(\mathbf{H}, \Omega)}^{\text{avg}} \\ &\leq e^{\frac{1}{2}(1+\beta T)} \|\mathbf{e}(\cdot, 0)\|_{(\mathbf{H}, \Omega)} + T \|\Pi_M(\mathcal{L}\{\mathbf{q}' - \mathbf{q}'_h\})(\cdot, T)\|_{(\mathbf{H}, \Omega)}^{\text{avg}} \\ &\quad + T \|\mathcal{L}\{\Pi_M(\mathbf{q}' - \mathbf{q}'_h)\}(\cdot, T)\|_{(\mathbf{H}, \Omega)}^{\text{avg}} + T \|\{\Pi_M(\mathcal{L} \mathbf{q}'_h) - \mathcal{L}(\Pi_M \mathbf{q}'_h)\}(\cdot, T)\|_{(\mathbf{H}, \Omega)}^{\text{avg}}. \end{aligned} \tag{76}$$

Substituting (76) into (75) gives (72). □

Table I. Nomenclature for the terms present in the error estimate (77).

Term	Name	Symbol
$\ (\mathbf{q}' - \mathbf{q}'_M)(\cdot, T)\ _{(\mathbf{H}, \Omega)}$	ROM solution error	ε_{ROM}
$\ \mathbf{e}(\cdot, 0)\ _{(\mathbf{H}, \Omega)}$	Initial ROM subspace error	ε_0
$\ (\mathbf{q}'_h - \Pi_M \mathbf{q}'_h)(\cdot, T)\ _{(\mathbf{H}, \Omega)}$	CFD representation error	ε_{rep}
$\ \{\Pi_M(\mathcal{L} \mathbf{q}'_h) - \mathcal{L}(\Pi_M \mathbf{q}'_h)\}(\cdot, T)\ _{(\mathbf{H}, \Omega)}^{\text{avg}}$	CFD operator representation error	$\varepsilon_{L\text{rep}}$
$\ (\mathbf{q}' - \mathbf{q}'_h)(\cdot, T)\ _{(\mathbf{H}, \Omega)}$	CFD solution error	ε_{CFD}
$\ \Pi_M(\mathcal{L}\{\mathbf{q}' - \mathbf{q}'_h\})(\cdot, T)\ _{(\mathbf{H}, \Omega)}^{\text{avg}} + \ \mathcal{L}\{\Pi_M(\mathbf{q}' - \mathbf{q}'_h)\}(\cdot, T)\ _{(\mathbf{H}, \Omega)}^{\text{avg}}$	CFD operator error	ε_L
$e^{\frac{1}{2}(1+\beta T)} \varepsilon_0 + \varepsilon_{\text{rep}} + T \varepsilon_{L\text{rep}} + 2\varepsilon_{\text{CFD}} + T \varepsilon_L$	Total error estimate	ε_{tot}

Let us analyze the estimate (72), repeated below for clarification and emphasis:

$$\begin{aligned}
 \underbrace{\|(\mathbf{q}' - \mathbf{q}'_M)(\cdot, T)\|_{(\mathbf{H}, \Omega)}}_{\varepsilon_{\text{ROM}}} &\leq e^{\frac{1}{2}(1+\beta T)} \underbrace{\|\mathbf{e}(\cdot, 0)\|_{(\mathbf{H}, \Omega)}}_{\varepsilon_0} + \underbrace{\|(\mathbf{q}'_h - \Pi_M \mathbf{q}'_h)(\cdot, T)\|_{(\mathbf{H}, \Omega)}}_{\varepsilon_{\text{rep}}} \\
 &\quad + T \underbrace{\|\{\Pi_M(\mathcal{L} \mathbf{q}'_h) - \mathcal{L}(\Pi_M \mathbf{q}'_h)\}(\cdot, T)\|_{(\mathbf{H}, \Omega)}^{\text{avg}}}_{\varepsilon_{L\text{rep}}} + 2 \underbrace{\|(\mathbf{q}' - \mathbf{q}'_h)(\cdot, T)\|_{(\mathbf{H}, \Omega)}}_{\varepsilon_{\text{CFD}}} \\
 &\quad + T \underbrace{\left[\|\Pi_M(\mathcal{L}\{\mathbf{q}' - \mathbf{q}'_h\})(\cdot, T)\|_{(\mathbf{H}, \Omega)}^{\text{avg}} + \|\mathcal{L}\{\Pi_M(\mathbf{q}' - \mathbf{q}'_h)\}(\cdot, T)\|_{(\mathbf{H}, \Omega)}^{\text{avg}} \right]}_{\varepsilon_L}.
 \end{aligned}
 \tag{77}$$

The error terms comprising (77) are named in Table I for ease of reference.

The initial error ε_0 is the difference (57) between the ROM solution and the projection of the exact solution onto the POD subspace at time $t=0$. For non-uniform mean flow ($\beta \neq 0$), this ‘initial subspace error’ is amplified by the time-dependent factor $e^{\beta T/2}$. The last two terms in (77), $2\varepsilon_{\text{CFD}} + T \varepsilon_L$, are essentially estimates of the error in the CFD solution. These terms converge, provided the error in the CFD solution \mathbf{q}'_h relative to the exact solution \mathbf{q}' is bounded as the CFD mesh is refined. A consequence of the POD approach for model reduction is that the second term in (77), the ‘CFD representation error’ ε_{rep} , also converges: that is, $\Pi_M \mathbf{q}'_h \rightarrow \mathbf{q}'_h$ provided both N (the number of snapshots used in constructing the ROM) $\rightarrow \infty$ and M (the basis size) $\rightarrow \infty$.

It turns out that some additional analysis is required to show rigorously the convergence of the third term in (77), the ‘CFD operator representation error’ $\varepsilon_{L\text{rep}}$. As it stands, convergence of this term is not apparent. This is because in the POD approach, the ROM basis is constructed to represent well \mathbf{q}'_h , and *not* to represent $\mathcal{L} \mathbf{q}'_h$. Representing $\mathcal{L} \mathbf{q}'_h$ is nonetheless critical to the performance of the ROM. Recalling that, from the governing equations, $\mathcal{L} \mathbf{q}' = -d\mathbf{q}'/dt$, and characterizing the numerical time integration error for the CFD solution with time step increment Δt as $\mathcal{L} \mathbf{q}'_h = -d\mathbf{q}'_h/dt + \Delta t^r$ for some $r \geq 1$, it can be shown (Lemma 5.2.4) that as the time increment between CFD snapshots *and* the representation error of the snapshots by the POD basis both decrease to zero, $\varepsilon_{L\text{rep}}$ also converges conditionally.

Lemma 5.2.4

Let $\mathbf{q}'_h \in \mathcal{H}^h(\Omega)$ be the CFD solution, with time derivative $\dot{\mathbf{q}}'_h \equiv d\mathbf{q}'_h/dt$. Consider the case where P equally spaced CFD snapshots are used to construct the POD basis, with time increment Δt_p separating each snapshot, so that the time derivative of the CFD solution can be estimated using a stable polynomial approximation of the form

$$\dot{\mathbf{q}}'_h = \frac{1}{\Delta t_p^{P-1}} \sum_{j=1}^P g_j \mathbf{q}'_h{}^j + \mathcal{O}(\Delta t_p^{P-1}), \tag{78}$$

for some weights $g_j \in \mathbb{R}$, $j = 1, \dots, P$. Let $\Pi_M: \mathcal{H}(\Omega) \rightarrow \mathcal{H}^M(\Omega)$ be an orthogonal projection operator satisfying properties 1–6 of Section A.2 of the Appendix and characterize the numerical time integration error in the CFD solution by

$$\dot{\mathbf{q}}'_h + \mathcal{L}\mathbf{q}'_h = \mathcal{O}(\Delta t^r), \quad r \geq 1, \tag{79}$$

where Δt is the time step increment. Then

$$\begin{aligned} \|\{\Pi_M(\mathcal{L}\mathbf{q}'_h) - \mathcal{L}(\Pi_M\mathbf{q}'_h)\}(\cdot, T)\|_{(\mathbf{H},\Omega)}^{\text{avg}} &\leq \|\mathcal{L}\{\Pi_M\mathbf{q}'_h - \mathbf{q}'_h\}(\cdot, T)\|_{(\mathbf{H},\Omega)}^{\text{avg}} \\ &\quad + \frac{1}{\Delta t_p^{P-1}} \sum_{j=1}^P g_j \|\{\Pi_M\mathbf{q}'_h - \mathbf{q}'_h\}(\cdot, t_j)\|_{(\mathbf{H},\Omega)}^{\text{avg}} \\ &\quad + \max\{\mathcal{O}(\Delta t^r), \mathcal{O}(\Delta t_p^{P-1})\}. \end{aligned} \tag{80}$$

Proof

Note first the identity

$$\Pi_M(\mathcal{L}\mathbf{q}'_h) = \Pi_M(-\dot{\mathbf{q}}'_h + \dot{\mathbf{q}}'_h + \mathcal{L}\mathbf{q}'_h) = -\Pi_M\dot{\mathbf{q}}'_h + \Pi_M(\dot{\mathbf{q}}'_h + \mathcal{L}\mathbf{q}'_h). \tag{81}$$

One also has that

$$\begin{aligned} \mathcal{L}(\Pi_M\mathbf{q}'_h) &= \mathcal{L}(\Pi_M\mathbf{q}'_h - \mathbf{q}'_h + \mathbf{q}'_h) \\ &= \mathcal{L}(\Pi_M\mathbf{q}'_h - \mathbf{q}'_h) + \mathcal{L}\mathbf{q}'_h \\ &= \mathcal{L}(\Pi_M\mathbf{q}'_h - \mathbf{q}'_h) - \dot{\mathbf{q}}'_h + (\dot{\mathbf{q}}'_h + \mathcal{L}\mathbf{q}'_h) \\ &= \mathcal{L}(\Pi_M\mathbf{q}'_h - \mathbf{q}'_h) - \dot{\mathbf{q}}'_h + \mathcal{O}(\Delta t^r). \end{aligned} \tag{82}$$

where $\mathcal{O}(\Delta t^r)$ with $r \geq 1$ is a measure of the projection of the temporal error in the CFD solution, which depends on the time step used in the CFD calculation and the order r of the CFD time integration scheme. Taking the norm of the difference between (82) and (81), applying the triangle inequality and invoking the fact that $\|\Pi_M\|_{(\mathbf{H},\Omega)}^{\text{avg}} = 1$ (Section A.2 of the Appendix) gives

$$\begin{aligned} \|\Pi_M(\mathcal{L}\mathbf{q}'_h) - \mathcal{L}(\Pi_M\mathbf{q}'_h)\|_{(\mathbf{H},\Omega)}^{\text{avg}} &= \|\mathcal{L}(\Pi_M\mathbf{q}'_h - \mathbf{q}'_h) + \Pi_M\dot{\mathbf{q}}'_h - \dot{\mathbf{q}}'_h - \Pi_M(\dot{\mathbf{q}}'_h + \mathcal{L}\mathbf{q}'_h) + \mathcal{O}(\Delta t^r)\|_{(\mathbf{H},\Omega)}^{\text{avg}} \\ &\leq \|\mathcal{L}(\Pi_M\mathbf{q}'_h - \mathbf{q}'_h)\|_{(\mathbf{H},\Omega)}^{\text{avg}} + \|\Pi_M\dot{\mathbf{q}}'_h - \dot{\mathbf{q}}'_h\|_{(\mathbf{H},\Omega)}^{\text{avg}} \\ &\quad + \|\Pi_M\|_{(\mathbf{H},\Omega)}^{\text{avg}} \|\dot{\mathbf{q}}'_h - \mathcal{L}\mathbf{q}'_h\|_{(\mathbf{H},\Omega)}^{\text{avg}} + \mathcal{O}(\Delta t^r) \\ &\leq \|\mathcal{L}(\Pi_M\mathbf{q}'_h - \mathbf{q}'_h)\|_{(\mathbf{H},\Omega)}^{\text{avg}} + \|\Pi_M\dot{\mathbf{q}}'_h - \dot{\mathbf{q}}'_h\|_{(\mathbf{H},\Omega)}^{\text{avg}} + \mathcal{O}(\Delta t^r). \end{aligned} \tag{83}$$

Consider the case where P equally spaced CFD snapshots are used to construct the POD basis, with time increment Δt_p separating each snapshot, so that the time derivative of the CFD solution can be estimated using a polynomial approximation of the form (78). The projection of this approximation onto $\mathcal{H}^M(\Omega)$ is

$$\Pi_M \dot{\mathbf{q}}'_h = \frac{1}{\Delta t_p^{P-1}} \sum_{j=1}^P g_j \Pi_M \mathbf{q}'_h{}^j + \mathcal{O}(\Delta t_p^{P-1}). \tag{84}$$

Taking the difference between (84) and $\dot{\mathbf{q}}'_h$:

$$\Pi_M \dot{\mathbf{q}}'_h - \dot{\mathbf{q}}'_h = \frac{1}{\Delta t_p^{P-1}} \sum_{j=1}^P g_j (\Pi_M \mathbf{q}'_h{}^j - \mathbf{q}'_h{}^j) + \mathcal{O}(\Delta t_p^{P-1}). \tag{85}$$

Substituting (85) into (83) and applying the triangle inequality gives (80). □

Lemma 5.2.4 implies a conditional convergence of the ‘CFD operator representation error’ $\mathcal{E}_{L_{\text{rep}}}$. The expression $\mathcal{L}(\Pi_M \mathbf{q}'_h - \mathbf{q}'_h)$ in (83) converges to zero as the size of the POD basis increases to infinity; the $\mathcal{O}(\Delta t^r)$ term converges to zero as the CFD time step decreases to zero. The remaining term in (83), $\Pi_M \dot{\mathbf{q}}'_h - \dot{\mathbf{q}}'_h$, is now required to converge. From Equation (85), one can see that this term is bounded provided that the numerator of the first term on the right-hand side of (85) is kept sufficiently small as the snapshot interval (the denominator) goes to zero. If this holds, the projection of the time derivative converges as both the time increment between CFD snapshots decreases to zero *and* as the representation error of the snapshots by the POD basis decreases to zero (that is, as the size of the basis increases to infinity).

Remark 2

The ‘conditional convergence’ of the $\Pi_M \dot{\mathbf{q}}'_h - \dot{\mathbf{q}}'_h$ term is of the same type of result as obtained by Kunisch and Volkwein [20, Corollary 4.9]. One may obtain a stronger convergence result by taking snapshots of the time derivative $\dot{\mathbf{q}}'$ in the construction of the ROM, an approach considered in [20]. In that case, $\|\Pi_M \dot{\mathbf{q}}'_h - \dot{\mathbf{q}}'_h\|_{(\mathbf{H},\Omega)}^{\text{avg}} \rightarrow 0$ as $N, M \rightarrow \infty$ just like $\varepsilon_{\text{rep}} \rightarrow 0$ as $N, M \rightarrow \infty$ as a direct consequence of the POD approach. The ROM proposed herein does not involve taking snapshots of the $\dot{\mathbf{q}}'$ field, and so the conditional convergence implied by (85) is inevitable given the current formulation. We emphasize, however, that there is nothing that precludes one from constructing the ROM by taking snapshots of the time-derivatives as well if one desires to obtain the stronger convergence result.

The boundedness of the right-hand side of (77) implies convergence of $\mathbf{q}' \rightarrow \mathbf{q}'_M$ in the (\mathbf{H}, Ω) -norm, with error estimate (77). This estimate is computable, provided an *a posteriori* estimator of the error in the CFD solution \mathbf{q}'_h relative to the exact solution \mathbf{q}' is available (Section 6).

6. NUMERICAL RESULTS

The convergence estimates of the previous section are now examined using a ROM constructed from CFD solutions of an IBVP for which an exact solution is known. The problem is the propagation and reflection from two parallel walls of a cylindrical acoustic pulse in a uniform

mean flow. The mean flow velocity is taken to be uniform in the x -direction with the Mach number $M_\infty \equiv \bar{u}/\bar{c} = 0.25$. The initial condition at time $t = 0$ is

$$\frac{p'}{\bar{\rho}\bar{c}^2} = 0.1M_\infty^2 \exp\{-(x-x_0)^2 - (y-y_0)^2\}, \quad \frac{\zeta'}{\bar{\zeta}} = -\frac{p'}{\bar{\rho}\bar{c}^2}, \quad u' = v' = w' = 0, \quad (86)$$

with $(x_0, y_0) = (10, -1)$. The exact solution for this IBVP can be found in [39]. The numerical solution was computed on a 3D rectangular prism domain, with extent $0 \leq x \leq 20$, $-5 \leq y \leq 5$, $0 \leq z \leq 1$. The grid was composed of approximately 212 000 nodes that were interconnected to form unstructured tetrahedral elements. Slip wall boundary conditions were applied on the constant y and z boundaries. The AERO-F node-centered finite volume code [40] was used to generate the time-accurate CFD solutions. The CFD simulation was run for a non-dimensional time of $T_{\text{tot}} = 6.4$ using 624 time steps. Snapshots were saved every four time steps beginning at time $t = t_0 = 0.57$ and ending at $t = T_{\text{tot}}$, and these were used to generate a fourteen-mode POD basis.

The ROMs were built by projecting the linearized Euler equations onto the POD basis using the symmetry inner product (26). The CFD snapshots and the resulting POD modes were represented using piece-wise linear tetrahedral finite elements and all projection inner products were computed using exact quadratures of these representations. This approach, described in detail in [21], ensures that the stability results of the present analysis are preserved by the discrete implementation. The ROMs were integrated in time using a fourth order Runge-Kutta scheme with the same time step that was used in the CFD computation. It was found through numerical experimentation that this time step was small enough to ensure the time step independence of the ROM solutions.

Figure 1 shows the pressure field at time $t - t_0 = 5.0$ for the CFD solution, compared with solutions reconstructed from six- and fourteen-mode ROM solutions. For this solution time the pulse has reflected from the bottom wall and is beginning to reflect from the top wall. The six-mode ROM solution shows significant differences from the CFD solution, whereas the fourteen-mode ROM solution is very nearly indistinguishable from the CFD solution.

The error terms appearing in (77) were computed using the available exact solution, the CFD solution and the ROM solution. Terms involving integration in time were approximated using the trapezoidal rule for numerical integration. Figure 2 shows the error estimates for the six-mode ROM and the fourteen-mode ROM, compared with the actual ROM solution error. The ROM solution error is well below the total error estimate for the entire time history. The conservative nature of the total error estimate is traced primarily to the ‘operator representation error’ term. For the six-mode ROM, the ROM solution error is well above the CFD solution error and tracks reasonably well with the CFD representation error. As the number of basis functions increases to fourteen, the ROM solution error drops below the CFD solution error term. The CFD representation error is reduced by about two orders of magnitude from the six-mode case, whereas the operator representation error drops only by about a factor of approximately three. The operator representation error evidently does not prohibit the ROM solution error from approaching the CFD solution error, however. We note, for clarity, that the CFD and ROM errors in Figure 2(b) are not constant as they appear; rather, these errors increase very slightly over the time interval studied.

Figure 3 shows the average error (expressed in the $\|\cdot\|_{(\mathbf{H}, \Omega)}^{\text{avg}}$ norm) of the ROM solution as a function of the basis size used to construct the ROM. The ROM solution error approaches the CFD solution error as the basis size increases, leveling out close to the CFD error. This result confirms the intuitive argument that a ROM can only be as accurate as the CFD solutions used to construct it. It also demonstrates that, given a sufficiently rich POD basis, the present projection

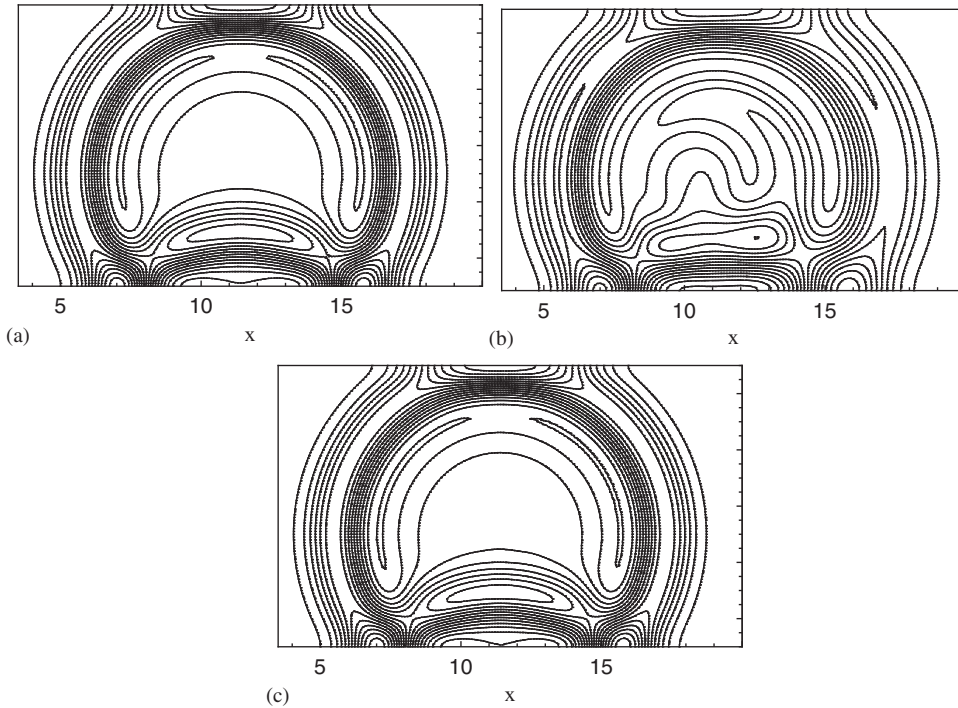


Figure 1. Pressure field at time $t - t_0 = 5.0$: (a) CFD solution; (b) six-mode ROM solution; and (c) fourteen-mode ROM solution.

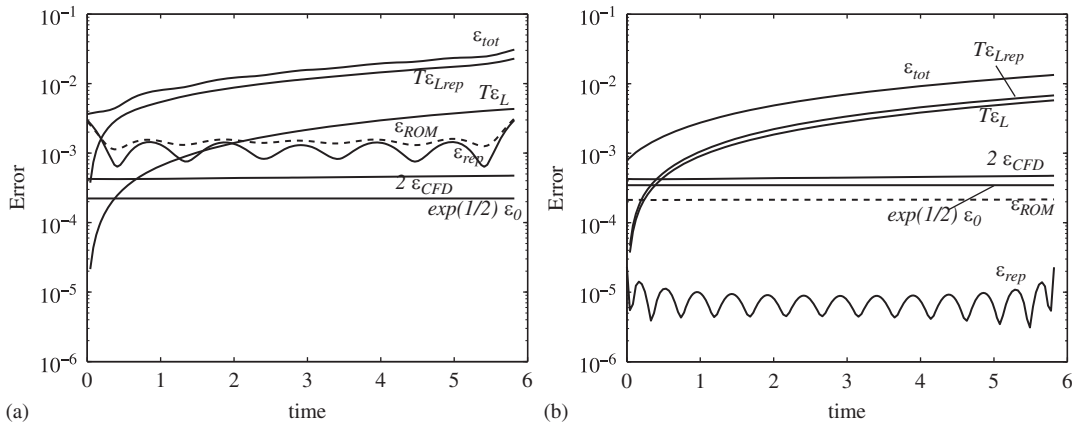


Figure 2. Error estimates and ROM solution error (broken line): (a) Six-mode ROM and (b) fourteen-mode ROM.

approach is capable of recovering the accuracy of the original CFD model. Interestingly, the ROM error is slightly lower than the CFD solution error when twelve or fourteen modes are used. This seemingly counterintuitive result is not inconsistent with the POD/Galerkin approach for model

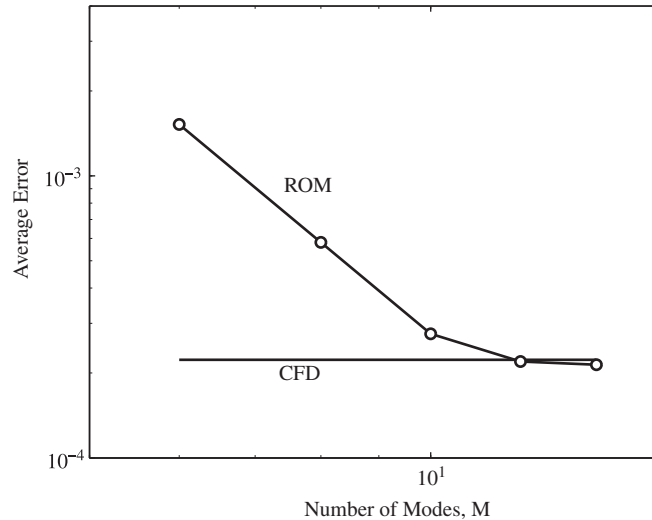


Figure 3. Error $\|\mathbf{q}'_M - \mathbf{q}'\|_{(\mathbf{H}, \Omega)}^{\text{avg}}$ in the ROM solution as a function of basis size, compared with the error $\|\mathbf{q}'_h - \mathbf{q}'\|_{(\mathbf{H}, \Omega)}^{\text{avg}}$ in the CFD solution error.

reduction. The POD basis forms an approximation for the CFD solution space, and the ROM solution necessarily lies in this space. However, the CFD solution trajectory through this space is not necessarily the best one. The projection can (and does for a twelve or fourteen mode ROM) give a solution trajectory through the space that is slightly closer to the exact solution. This suggests that a slightly more accurate ROM may result from projecting the original continuous equations rather than projecting the discretized equations. It is not clear, however, whether this result is general or specific to our particular test case.

7. CONCLUSIONS

A reduced order model (ROM) for the compressible, linearized Euler equations, based on the proper orthogonal decomposition (POD)/Galerkin projection method, has been developed and tested. In the proposed model reduction technique, the Galerkin projection step is applied to the original continuous equations, rather than their discretized analogs. A symmetry inner product is defined such that the application of the Galerkin projection method in this inner product is guaranteed to produce stable ROMs for the governing fluid equations. It is shown that both the formulation of the initial boundary value problem (IBVP) of interest and the choice of inner product used in the Galerkin projection step are crucial to stability and convergence of the ROM. Sufficient conditions for well-posed and stable boundary conditions on the far-field and solid wall boundaries are stated and proven. A non-reflecting far-field and acoustically reflecting solid wall boundary treatment is developed such that numerical stability of the entire Galerkin scheme with boundary conditions is preserved. The specific penalty-like formulation that arises in the application of these boundary conditions motivates a convergence estimate analysis resembling the analysis in [22] and leads to *a priori* error bounds for the ROM solution. The derived error estimates are computed for the

test case of a cylindrically propagating and reflecting acoustic pulse, for which an exact solution is available. The ROM solution error remains bounded by the estimates, which for this test case gives conservative estimates. The average ROM solution error converges to slightly below the average CFD solution error as the ROM basis size is increased, indicating that for a sufficiently rich basis the present approach is capable of giving an accurate and stable representation of the full CFD model. The primary accomplishment of this work is the mathematically rigorous analysis of the numerical properties of a ROM for compressible flow. This analysis leads to a much better understanding of these properties and places issues such as stability and convergence of the ROM on a firmer mathematical footing.

APPENDIX A

A.1. Diagonalization of \mathbf{A}_n

Let $\mathbf{A}_n \equiv \mathbf{A}_1 n_1 + \mathbf{A}_2 n_2 + \mathbf{A}_3 n_3$. The matrices \mathbf{S} that diagonalize \mathbf{A}_n (so that $\mathbf{A}_n = \mathbf{S} \mathbf{\Lambda}_n \mathbf{S}^{-1}$, with $\mathbf{\Lambda}_n$ given in (9)) are:

$$\mathbf{S} = \begin{pmatrix} 0 & n_3 & n_2 & \frac{1}{2}n_1 & -\frac{1}{2}n_1 \\ n_3 & 0 & -n_1 & \frac{1}{2}n_2 & -\frac{1}{2}n_2 \\ -n_2 & -n_1 & 0 & \frac{1}{2}n_3 & -\frac{1}{2}n_3 \\ n_1 & -n_2 & n_3 & -\frac{\bar{\zeta}}{2\bar{c}} & -\frac{\bar{\zeta}}{2\bar{c}} \\ 0 & 0 & 0 & \frac{\gamma\bar{p}}{2\bar{c}} & \frac{\gamma\bar{p}}{2\bar{c}} \end{pmatrix}, \quad \mathbf{S}^{-1} = \begin{pmatrix} 0 & n_3 & -n_2 & n_1 & \frac{\bar{\zeta}}{\gamma\bar{p}}n_1 \\ n_3 & 0 & -n_1 & -n_2 & -\frac{\bar{\zeta}}{\gamma\bar{p}}n_2 \\ n_2 & -n_1 & 0 & n_3 & \frac{\bar{\zeta}}{\gamma\bar{p}}n_3 \\ n_1 & n_2 & n_3 & 0 & \frac{\bar{c}}{\gamma\bar{p}} \\ -n_1 & -n_2 & -n_3 & 0 & \frac{\bar{c}}{\gamma\bar{p}} \end{pmatrix}. \quad (\text{A1})$$

It follows that

$$\mathbf{v}' \equiv \mathbf{S}^{-1} \mathbf{q}' = \begin{pmatrix} (n_3 u'_2 - n_2 u'_3 + n_1 \zeta') + \frac{\bar{\zeta}}{\gamma\bar{p}} n_1 p' \\ (n_3 u'_1 - n_1 u'_3 - n_2 \zeta') - \frac{\bar{\zeta}}{\gamma\bar{p}} n_2 p' \\ (n_2 u'_1 - n_1 u'_2 + n_3 \zeta') + \frac{\bar{\zeta}}{\gamma\bar{p}} n_3 p' \\ u'_n + \frac{\bar{\zeta}}{\bar{c}} p' \\ -u'_n + \frac{\bar{\zeta}}{\bar{c}} p' \end{pmatrix}$$

$$= \begin{pmatrix} \sum_{k=1}^M \left[n_1 \left(\phi_k^4 + \left(\frac{\bar{\zeta}}{c} \right)^2 \phi_k^5 \right) - n_2 \phi_k^3 + n_3 \phi_k^2 \right] a_k(t) \\ \sum_{k=1}^M \left[-n_1 \phi_k^3 - n_2 \left(\phi_k^4 + \left(\frac{\bar{\zeta}}{c} \right)^2 \phi_k^5 \right) + n_3 \phi_k^1 \right] a_k(t) \\ \sum_{k=1}^M \left[-n_1 \phi_k^2 + n_2 \phi_k^1 + n_3 \left(\phi_k^4 + \left(\frac{\bar{\zeta}}{c} \right)^2 \phi_k^5 \right) \right] a_k(t) \\ \sum_{k=1}^M \left[n_1 \phi_k^1 + n_2 \phi_k^2 + n_3 \phi_k^3 + \frac{\bar{\zeta}}{c} \phi_k^5 \right] a_k(t) \\ \sum_{k=1}^M \left[-n_1 \phi_k^1 - n_2 \phi_k^2 - n_3 \phi_k^3 + \frac{\bar{\zeta}}{c} \phi_k^5 \right] a_k(t) \end{pmatrix}, \tag{A2}$$

where $\phi_k^T \equiv (\phi_k^1 \ \phi_k^2 \ \phi_k^3 \ \phi_k^4 \ \phi_k^5) \in \mathbb{R}^5$ is the ROM basis vector.

A.2. Projection operator

Let \mathcal{V} and \mathcal{V}^M be vector spaces. By definition, a projection operator $\Pi_M: \mathcal{V} \rightarrow \mathcal{V}^M$ has the following properties:

1. For all $u \in \mathcal{V}$, $\Pi_M(\Pi_M u) = \Pi_M u$ (that is, Π_M is *idempotent*).
2. For all $u, v \in \mathcal{V}$, $\Pi_M(u + v) = \Pi_M u + \Pi_M v$ (that is, Π_M is *linear*).
3. $\|\Pi_M\| = 1$ for any norm $\|\cdot\|$ on \mathcal{V} (a consequence 1. above).
4. For all $u \in \mathcal{V}$, $\partial(\Pi_M u) / \partial t = \Pi_M(\partial u / \partial t)$ (that is, Π_M is a spatial-only operator, so time-differentiation commutes with projection).
5. For all $v \in \mathcal{V}^M$, $\Pi_M v = v$.
6. For all $v \in (\mathcal{V}^M)^\perp$, $\Pi_M v = 0$ (here $(\mathcal{V}^M)^\perp$ denotes the subspace orthogonal to \mathcal{V}^M).

A.3. Well-posedness

Consider a general IBVP of the form

$$\begin{aligned} \frac{\partial u}{\partial t} &= Pu + F, \quad t \geq 0, \\ Bu &= g, \\ u &= f, \quad t = 0, \end{aligned} \tag{A3}$$

Here, P is a differential operator in space, and B is a boundary operator acting on the solution at the spatial boundary.

Definition 2.8 in [35]: The IBVP (A3) is *well-posed* if for $F = 0, g = 0$, there is a unique solution satisfying $\|u(\cdot, t)\| \leq K e^{\beta t} \|f(\cdot)\|$, where K and β are constants independent of $f(x)$.

A.4. Stability

Consider the following semi-discrete problem:

$$\begin{aligned} \frac{du_j}{dt} &= Qu_j + F_j, \quad j=1, 2, \dots, N-1, \\ B_h u &= g(t), \\ u_j(0) &= f_j, \quad j=1, 2, \dots, N, \end{aligned} \tag{A4}$$

where Q is a discretizing operator, F_j and f_j are the discretized version of F and f , respectively, and $B_h u$ denotes the complete set of discretized boundary conditions. Let $\|\cdot\|_h$ be a discrete norm.

Definition 2.11 in [35]: The semi-discrete IBVP (A4) is *stable* if there is a unique solution satisfying $\|u(\cdot, t)\|_h \leq Ke^{\beta t} \|f(\cdot)\|_h$, where K and β are constants independent of f and g .

A.5. Proof of Theorem 4.3.1

By Definition 2.8 in [35], to show well-posedness of (13), it is sufficient to show that the energy of the analogous homogeneous IBVP is bounded in some valid norm. Selecting the (\mathbf{H}, Ω) -norm:

$$\begin{aligned} \frac{1}{2} \frac{d}{dt} \|\mathbf{q}'\|_{(\mathbf{H}, \Omega)}^2 &= \frac{1}{2} \frac{d}{dt} \int_{\Omega} \mathbf{q}'^T \mathbf{H} \mathbf{q}' \, d\Omega \\ &= \int_{\Omega} \mathbf{q}'^T \mathbf{H} \frac{\partial \mathbf{q}'}{\partial t} \, d\Omega \\ &= - \int_{\Omega} \mathbf{q}'^T \mathbf{H} \left[\mathbf{A}_i \frac{\partial \mathbf{q}'}{\partial x_i} + \mathbf{C} \mathbf{q}' \right] \, d\Omega \\ &= - \frac{1}{2} \int_{\Omega} \left[\frac{\partial}{\partial x_i} (\mathbf{q}'^T \mathbf{H} \mathbf{A}_i \mathbf{q}') - \mathbf{q}'^T \frac{\partial (\mathbf{H} \mathbf{A}_i)}{\partial x_i} + 2 \mathbf{q}'^T \mathbf{H} \mathbf{C} \right] \mathbf{q}' \, d\Omega \\ &= - \frac{1}{2} \int_{\Omega} \frac{\partial}{\partial x_i} (\mathbf{q}'^T \mathbf{H} \mathbf{A}_i \mathbf{q}') \, d\Omega + \frac{1}{2} \int_{\Omega} \mathbf{q}'^T \left[\frac{\partial (\mathbf{H} \mathbf{A}_i)}{\partial x_i} - \mathbf{H} \mathbf{C} - \mathbf{C}^T \mathbf{H} \right] \mathbf{q}' \, d\Omega \\ &= - \frac{1}{2} \int_{\partial \Omega} \mathbf{q}'^T \mathbf{H} \mathbf{A}_n \mathbf{q}' \, dS + \frac{1}{2} \int_{\Omega} \mathbf{q}'^T \mathbf{H}^{T/2} \mathbf{B} \mathbf{H}^{1/2} \mathbf{q}' \, d\Omega \\ &\leq - \frac{1}{2} \int_{\partial \Omega_w} \mathbf{q}'^T_{w0} \mathbf{H} \mathbf{A}_n \mathbf{q}'_{w0} \, dS - \frac{1}{2} \int_{\partial \Omega_F} \mathbf{q}'^T_{f0} \mathbf{H} \mathbf{A}_n \mathbf{q}'_{f0} \, dS + \frac{1}{2} \beta \int_{\Omega} \mathbf{q}'^T \mathbf{H} \mathbf{q}' \, d\Omega, \end{aligned} \tag{A5}$$

where \mathbf{B} is defined in (34) and β is an upper bound on the eigenvalues of \mathbf{B} . By (27),

$$\begin{aligned} - \frac{1}{2} \int_{\partial \Omega_w} \mathbf{q}'^T_{w0} \mathbf{H} \mathbf{A}_n \mathbf{q}'_{w0} \, dS - \frac{1}{2} \int_{\partial \Omega_F} \mathbf{q}'^T_{f0} \mathbf{H} \mathbf{A}_n \mathbf{q}'_{f0} \, dS &= - \frac{1}{2} \int_{\partial \Omega_F} \mathbf{v}'^T_{f0} \mathbf{Q} \mathbf{A}_n \mathbf{v}'_{f0} \, dS \\ &\quad - \frac{1}{2} \int_{\partial \Omega_w} \mathbf{v}'^T_{w0} \mathbf{Q} \mathbf{A}_n \mathbf{v}'_{w0} \, dS, \end{aligned} \tag{A6}$$

where $\mathbf{v}'_{f0} = \mathbf{S}\mathbf{q}'_{f0}$ and similarly for \mathbf{v}'_{w0} . It follows from the property that \mathbf{Q} is symmetric positive definite and $\mathbf{Q}\mathbf{\Lambda}_n = \mathbf{\Lambda}_n\mathbf{Q}$ that

$$\mathbf{v}'^T \mathbf{Q}\mathbf{\Lambda}_n \mathbf{v}' = \mathbf{Q}^{T/2} [\mathbf{v}'^T \mathbf{\Lambda}_n \mathbf{v}'] \mathbf{Q}^{1/2} = (\mathbf{Q}^{1/2})^T \left[\sum_{i=1}^5 \lambda_i (v'_i)^2 \right] \mathbf{Q}^{1/2}. \quad (\text{A7})$$

If the conditions (32) hold, the last line of (A5) thus reduces to

$$\frac{d}{dt} \|\mathbf{q}'\|_{(\mathbf{H},\Omega)}^2 \leq \beta \|\mathbf{q}'\|_{(\mathbf{H},\Omega)}^2. \quad (\text{A8})$$

Applying Gronwall's lemma to (A8) gives (33).

ACKNOWLEDGEMENTS

This research was funded by Sandia National Laboratories Laboratory Directed Research and Development (LDRD) program. Sandia is a multiprogram laboratory operated by Sandia Corporation, a Lockheed Martin Company for the United States Department of Energy's National Nuclear Security Administration under contract DE-AC04-94AL85000. The first author acknowledges the support of an NDSEG Fellowship sponsored by the U.S. Department of Defense, and also the support of a National Physical Science Consortium (NPSC) Fellowship, funded by the Engineering Sciences Center at Sandia National Laboratories.

REFERENCES

1. Nguyen NC, Rozza G, Patera AT. Reduced basis approximation and a posteriori error estimation for the time-dependent viscous Burgers equation. *Calcolo* 2009; **46**(3):157–185.
2. Veroy K, Prud'homme C, Patera AT. Reduced-basis approximation of the viscous Burgers equation: rigorous a posteriori error bounds. *Comptes Rendus de l'Academie des Sciences, Serie I* 2003; **337**(9):619–624.
3. Veroy K, Prud'homme C, Rowas DV, Patera AT. A posteriori error bounds for reduced-basis approximation of parametrized noncoercive and nonlinear elliptic partial differential equations. *Proceedings of the 16th AIAA Computational Fluid Dynamics Conference, AIAA 2003-3847*, Orlando, FL, 2003.
4. Veroy K, Patera AT. Certified real-time solution of the parametrized steady incompressible Navier–Stokes equations: rigorous reduced-basis a posteriori error bounds. *International Journal for Numerical Methods in Fluids* 2005; **47**:773–788.
5. Rowley CW. Model reduction for fluids, using balanced proper orthogonal decomposition. *International Journal of Bifurcation and Chaos* 2005; **15**(3):997–1013.
6. Willcox K, Peraire J. Balanced model reduction via the proper orthogonal decomposition. *AIAA Journal* 2002; **40**(11):2323–2330.
7. Bui-Thanh T, Willcox K, Ghattas O. Model reduction for large-scale systems with high-dimensional parametric input space. *SIAM Journal on Scientific Computing* 2008; **30**(6):3270–3288.
8. Taylor JA, Glauser MN. Towards practical flow sensing and control via POD and LSE based low-dimensional tools. *Journal of Fluids Engineering* 2003; **126**(3):337–345.
9. LeGresley PA, Alonso JJ. Investigation of non-linear projection for POD based reduced order models for aerodynamics. *AIAA 39th Aerospace Science Meeting and Exhibit, AIAA 2001-0926*, Reno, NV, 2001.
10. Hall KC, Thomas JP, Dowell EH. Proper orthogonal decomposition technique for transonic unsteady aerodynamic flows. *AIAA Journal* 2000; **38**(10):1853–1862.
11. Lieu T, Farhat C, Lesoinne M. Reduced-order fluid/structure modeling of a complete aircraft configuration. *Computer Methods in Applied Mechanics and Engineering* 2006; **195**:5730–5742.
12. Aubry N, Holmes P, Lumley J, Stone E. The dynamics of coherent structures in the wall region of a turbulent boundary layer. *Journal of Fluid Mechanics* 1988; **192**:115–173.
13. Holmes P, Lumley JL, Berkooz G. *Turbulence, Coherent Structures, Dynamical Systems and Symmetry*. Cambridge University Press: New York, NY, 1996.

14. Sirovich L. Turbulence and the dynamics of coherent structures, part III: dynamics and scaling. *Quarterly of Applied Mathematics* 1987; **45**(3):583–590.
15. Bui-Thanh T, Willcox K, Ghattas O, van Bloemen Waanders B. Goal-oriented, model-constrained optimization for reduction of large-scale systems. *Journal of Computational Physics* 2007; **224**:880–896.
16. Bai Z, Dewilde PM, Freund RW. Reduced order modeling. In *Numerical Methods in Electromagnetics, Handbook of Numerical Analysis*, Schilders WHA, ter Maton EJW (eds), vol. XIII. Elsevier: Amsterdam, 2005; 825–895.
17. Kwasniok F. Empirical low-order models of barotropic flow. *Journal of Atmospheric Sciences* 2004; **61**(2): 235–245.
18. Rathinam M, Petzold LR. A new look at proper orthogonal decomposition. *SIAM Journal on Numerical Analysis* 2003; **41**(5):1893–1925.
19. Kunisch K, Volkwein S. Galerkin proper orthogonal decomposition methods for parabolic problems. *Numerische Mathematik* 2001; **90**:117–148.
20. Kunisch K, Volkwein S. Galerkin proper orthogonal decomposition for a general equation in fluid dynamics. *SIAM Journal on Numerical Analysis* 2002; **40**(2):492–515.
21. Barone MF, Kalashnikova I, Segalman DJ, Thornquist HK. Stable Galerkin reduced order models for linearized compressible flow. *Journal of Computational Physics* 2009; **228**:1932–1946.
22. Funaro D, Gottlieb D. Convergence results for pseudospectral approximations of hyperbolic systems by a penalty-type boundary treatment. *Mathematics of Computation* 1991; **57**(196):585–596.
23. Lumley JL. *Stochastic Tools in Turbulence*. Academic Press: New York, NY, 1971.
24. Gustafsson B, Sundstrom A. Incompletely parabolic problems in fluid dynamics. *SIAM Journal on Applied Mathematics* 1978; **35**(2):343–357.
25. Oliger J, Sundstrom A. Theoretical and practical aspects of some initial boundary value problems in fluid dynamics. *SIAM Journal on Applied Mathematics* 1978; **35**(3):419–446.
26. Harten A. On the symmetric form of systems of conservation laws with entropy. *Journal of Computational Physics* 1983; **49**:151–164.
27. Hughes TJR, Franca LP, Mallet M. A new finite element formulation for computational fluid dynamics: I. Symmetric forms of the compressible Euler and Navier–Stokes equations and the second law of thermodynamics. *Computer Methods in Applied Mechanics and Engineering* 1986; **54**:223–234.
28. Bova SW, Carey GF. An entropy variable formulation and applications for the two-dimensional shallow water equations. *International Journal for Numerical Methods in Fluids* 1996; **23**:29–46.
29. Greven A, Keller G, Warnecke G. *Entropy*. Princeton University Press: Princeton, NJ, 2003.
30. Gustafsson B, Kreiss HO, Oliger J. *Time Dependent Problems and Difference Methods*. Wiley: New York, NY, 1995.
31. Abarbanel S, Gottlieb D. Optimal time splitting for two- and three-dimensional Navier–Stokes equations with mixed derivatives. *Journal of Computational Physics* 1981; **35**:1–33.
32. Barone MF, Payne JL. Methods for simulation-based analysis of fluid–structure interaction. SAND2005-6573, Sandia National Laboratories, Albuquerque, NM, 2005.
33. Barone MF, Kalashnikova I, Segalman DJ, Thornquist HK. Galerkin reduced order models for compressible flow with structural interaction. *AIAA 46th Aerospace Science Meeting and Exhibit, AIAA 2008-0612*, Reno, NV, 2008.
34. Barone MF, Kalashnikova I, Brake MR, Segalman DJ. Reduced order modeling of fluid/structure interaction. SAND2009-7189, Sandia National Laboratories Report, Sandia National Laboratories, Albuquerque, NM, 2009.
35. Gustafsson B. *High Order Difference Methods for Time Dependent PDE*. Springer: Leipzig, Germany, 2008.
36. Sirisup S, Karniadakis GE. Stability and accuracy of periodic flow solutions obtained by a POD-penalty method. *Physica D* 2005; **202**:218–237.
37. Hesthaven JS, Gottlieb D. A stable method for the compressible Navier–Stokes equations: I. Open boundary conditions. *SIAM Journal on Scientific Computing* 1996; **17**(3):579–612.
38. Bodony DJ. Analysis of sponge zones for computational fluid mechanics. *Journal of Computational Physics* 2006; **212**:681–702.
39. Tam CKW, Webb JC. Dispersion-relation-preserving finite difference schemes for computational acoustics. *Journal of Computational Physics* 1993; **107**:262–281.
40. Farhat C, Geuzaine P, Brown G. Application of a three-field nonlinear fluid–structure formulation to the prediction of the aeroelastic parameters of an F-16 fighter. *Computers and Fluids* 2003; **32**:3–29.